PRODUCTION OF POINT DEFECTS BY PLASTIC DEFORMATION IN COPPER

by

DAVID TSENG

A THESIS

SUBMITTED TO THE FACULTY OF GRADUATE STUDIES

IN PARTIAL FULFILMENT OF THE REQUIREMENTS FOR THE DEGREE

OF MASTER OF SCIENCE

DEPARTMENT OF MECHANICAL ENGINEERING

UNIVERSITY OF MANITOBA

WINNIPEG, MANITOBA

February, 1974

TABLE OF CONTENTS

LIST OF FIGURES

ACKNOWLEDGMENT

I wish to express my sincere thanks to Dr. K. Tangri for his patient guidance and constant encouragement throughout the course of this work.

The financial assistance from the University of Manitoba is gratefully acknowledged.

ABSTRACT

All the existing models of creation of point defects by moving dislocations have been reviewed. They are based on the geometrical model of edge dislocations. The models may be classified into (a) the recombination of edge dislocations and (b) climb of edge dislocations.

The concentration of point defects produced by cold-work depends on the deformation parameters. The important parameters are stress, strain, strain rate, and temperature of deformation.

The generation of point defects by tensile deformation in copper has been investigated by resistivity measurements. The fast increase in resistivity in the microstrain region is attributed to the operation of the dipole mechanism. For strains greater than 2.5%, the intersection mechanism is dominant. Saada's model has been re-examined. The length of the point defect string in each intersection event is insensitive to the size of the dislocation network. However, it depends on the average dislocation velocity. The concentration of point defects is given by

$$C = \frac{\text{const.}}{\mu^2 b} \int_0^{\varepsilon} \sigma^2 d\varepsilon$$

The concentration of point defects depends non-linearly on the strain rate. This is due to the combined effects of the athermal

cutting of attractive trees and the thermally activated non-conservative motion of jogs.

Two substages have been found in the stage III temperature range in cold-worked copper. The substages are not changed by the solute addition. The structure of stage IV depends sensitively on the solute atoms. These further confirm that the stage III defects are interstitials and the stage IV defects are vacancies.

1. INTRODUCTION AND OBJECTIVES

A point defect is a disturbance in a crystal of such a nature that it can be completely enclosed in a small sphere of a few atomic diameters in dimension. Only the structural point defects, namely vacancies and interstitials, will be discussed here. A vacancy is a vacant lattice site, and an interstitial is an atom located at a non-lattice site. Vacancies and interstitials are parts of the spectra of the elementary excitations in solids at temperatures above the absolute zero. Non-equilibrium condentration of point defects can be generated by plastic deformation, high energy particle bombardment, and a fast quench from high temperatures.

A wealth of information has been obtained in the past decade about the properties of point defects in FCC metals by the studies of self-diffusion, thermal equilibrium measurements, radiation damage, plastic deformation, and theoretical calculations. However, the understanding of the behaviour of point defects in cold-worked metals is still rudimentary because of the inherent complexities of the nature of deformed metals. To study the point defects in cold-worked metals one needs the data on the properties of vacancies and interstitials obtained from quenching and irradiation experiments. As such information compiled from these two types of experiments is summarized in the following sections.

1.1. QUENCHING AND IRRADIATION EXPERIMENTS

1.1.1. Quenching Experiments

It is known from thermodynamics[1] that the equilibrium concentration of point defect at temperature T is given by

$$C = e^{s/k} \cdot e^{-E_F/kT}, \qquad (1\text{-}1)$$

where E_F is the energy required to create a single defect and s is the entropy of formation which arises from the atomic and electronic relaxations around the defect. The theoretical estimate of the entropies of formation of vacancies and interstitials for a FCC lattice has been made by Huntington et al[3]. The entropy for an interstitial is 0.8K and that for a vacancy 1.47K. The energy of formation for an interstitial in copper is 3 eV[4] and that for a vacancy 1 eV[5, 6, 7]. The ratio of the concentrations of vacancies and interstitials in copper at temperatures near the melting point (say 1200°K) is approximately equal to

$$\frac{C_V}{C_I} = \frac{e^{1.47} \cdot e^{-1.6\cdot10^{-12}/1200K}}{e^{0.8} \cdot e^{-3\cdot1.6\cdot10^{-12}/1200K}} = e^{20} \simeq 5\cdot10^8$$

Thus the majority of defects obtained by quenching are vacancies. The interstitials can in general be neglected. However, quenching does not produce simple types of point defects. The analysis of quenching data is complicated by the formation of divacancies and larger vacancy clusters during quenching. The most reliable data

derived from quenching experiments are the energies of formation for monovacancies. A summary of the results is given in Table 1-1. There are three quenching parameters which influence the accuracy of the quenching results.

(1) The quenching temperature T_q

Too high a T_q will result in a high degree of clustering because of the high concentration of vacancies. Cotterill[34] has found large concentrations of stacking fault tetrahedra in gold specimens quenched from above 800°C. The tetrahedra are very stable and anneal out between 600 and 650°C which is well beyond the annealing temperatures for point defects.

(2) The quenching rate

A quench must be fast enough to freeze in a high percentage of vacancies. Since the quenching rate has a technical limit, the equilibrium concentration of vacancies at a given T_q can be obtained by varying the quenching rate and extrapolating the quenching rate to infinity[35].

(3) The quenching strain

A rapidly quenched specimen is always slightly strained because of the inhomogenous thermal contraction which is present when the outside of the specimen is cooled relative to the interior. The quenching stress induces plastic deformation which produces

Table 1-1 Energy of Formation for Monovacancies.

Metal	E_f (eV)	Reference
Gold	0.98±0.1	8
	0.98±0.03	9
	0.95±0.1	10
	0.79	11
	0.97±0.1	12
	0.98	13
	0.97	14
	0.98	15
	0.94±0.02	16
Platinum	1.4±0.1	10
	1.3±0.1	17
	1.4	36
	1.18	11
	1.51±0.04	19
Silver	1.10±0.04	20
	1.10±0.01	21
	1.06	22
	1.04±0.1	23
	1.0	36

Aluminum	0.76±0.04	17
	0.79±0.04	24
	0.76±0.03	37
	0.76	26
	0.73±0.03	27
Copper	1.0	28
	1.17±0.06	29
	1.14±0.06	30
Nickel	1.5±0.05	31
Tin	0.51±0.05	32
Magnesium	0.89±0.06	33

extra point defects and dislocations. To prevent the errors due to the quenching strain, the specimen diameter should be small.

1.1.2. Irradiation Experiments

The irradiation of a crystal with energetic particles produces equal amount of vacancies and interstitials. In the lowest energy (i.e. threshold) case, the collision of the incident particle with the lattice atom displaces the lattice atom to an interstitial site, leaving the original lattice site vacant. Such a vacancy-interstitial pair is called a Frenkel defect. The threshold energy is the minimum energy required to produce a stable Frenkel defect. The threshold energies for the noble metals are listed below[1]:

Metal	Threshold energy (eV)
Cu	19
Ag	28
Au	35

As the energy of the bombarding particles is increased, a number of Frenkel defects will be created per incident particle. Some of the lattice atoms can gain enough energy from the collision and further produces vacancy-interstitial pairs. The irradiation with the energetic heavy particles will create defect clusters as well as the heavily damaged regions called spikes. Such unwanted

complications can be avoided by using electron irradiation. This review is based on this type of experiments only. The Frenkel defects produced by electron irradiation can be divided into two groups. The first group are those bound Frenkel pairs in which the interstitial and vacancy have sufficient interaction. Upon warming up the specimen, the interstitial will migrate to the vacancy and annihilate each other. Such process requires the least thermal energy. The second group are the unbound defect pairs in which the vacancy and the interstitial do not have an interaction. Each point defect migrates independently during annealing at higher temperatures.

1.1.3. Annealing of Point Defects in Metals

Much of the knowledge about the properties of point defects has been obtained from the annealing experiments. On warming up the specimen, the thermal energy activates the migration of the point defects. The following processes can happen during annealing:

(1) An interstitial can migrate to a vacancy and annihilate each other;

(2) A point defect can be trapped by an impurity atom and be freed at higher annealing temperature;

(3) A point defect can migrate to sinks, such as free surfaces, grain boundaries, and dislocations;

(4) The point of the same type can form clusters and the clusters can dissociate at higher temperatures.

Several of the processes can happen at a given annealing temperature, which makes the analysis of the annealing data difficult. The reactions of point defects can be monitored by measuring the change in physical properties such as the electrical resistivity, the stored energy, and the hardness. The resistivity technique has high sensitivity and is the most widely used technique. It also leads to the present difficulties in this field which will be considered later.

The annealing of point defects is in general approached by the chemical rate equation of the form:

$$\frac{dC}{dt} = \alpha f(C), \tag{1-2}$$

where t and C are the time and concentration, respectively. The rate constant α can be written as $\alpha = \nu_o \exp(-E_m/kT)$, where ν_o is the frequency factor, E_m the activation energy for migration, and k the Boltzmann constant. The function f(C) depends on the type of reaction. The annilihation of close Frenkel pairs and the migration of point defects to sinks are equivalent to the mono-molecular chemical reaction. Eq. (1-2) becomes:

$$\frac{dC}{dt} = -\alpha C \tag{1-3}$$

The random annihiliation of vacancies and interstitials is described by:

$$\frac{dC}{dt} = -\alpha C^2 \qquad (1\text{-}4)$$

Eq. (1-2) is sometimes written as $dC/dt = -\alpha C^{\gamma}$, where γ is the reaction order. In other words, the function f(C) reflects the type of process occurring during annealing. However this information is not very specific, since in the actual case several processes can happen at a given temperature.

There are two different types of annealing experiments. (1) The isothermal annealing is performed at a constant temperature. The plot, ln(dC/dt) vs. C, gives the effective reaction order. The isothermal annealing is also used to determine the migration energy. The specimen is initially annealed at T_1. At a certain instant, the temperature is raised to T_2 (Fig. 1-1). The migration energy is immediately calculable from the reaction:

$$\ln\{(dC/dt)_1/(dC/dt)_2\} = -E_m/k\cdot(1/T_1 - 1/T_2) \qquad (1\text{-}5)$$

(2) The isochronal annealing is performed in such a way that the temperature is proportional to the annealing time,

$$T = ht, \qquad (1\text{-}6)$$

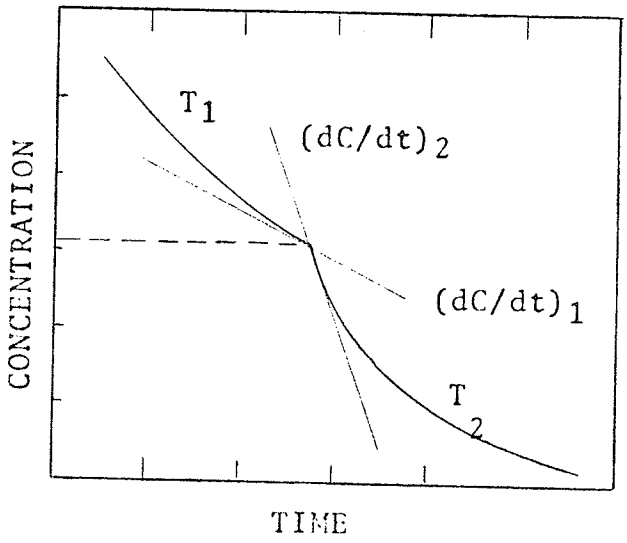

FIG. 1-1

where h is called the heating rate. The actual performing of the isochronal annealing is explained in Section 2.4. Whenever a group of defects anneal out within a temperature range, a step appears on the C versus T plot. Such a step is called an annealing stage. The identification of the point defect species active in each stage is the central problem of the isochronal annealing experiments. Very few data on the isochronal annealing of quenched metals are available because the extensive clustering of vacancies occurs during annealing. The isochronal annealing of irradiated FCC metals occurs in four main stages and several substages. Their representative characteristics and the interpretations proposed are listed below. The temperature ranges indicated are valid for the noble metals.

Stage I (0-60^{o}K)

This is the largest annealing stage in irradiated metals. About 85% of the irradiation induced resistivity recovers in copper (Fig. 1-2). There are five well-defined substages. Stage Ia has not been observed in Ag, Al and Ni (Fig. 1-3). The interpretations given by Corbett[38] et al are the following: Stages Ia, Ib, and Ic are due to the recombination of the bound Frenkel pairs. This interpretation is based on the following facts.

(1) The annealing kinetics of these stages obeys the first order reaction law given by Eq. (1-3),

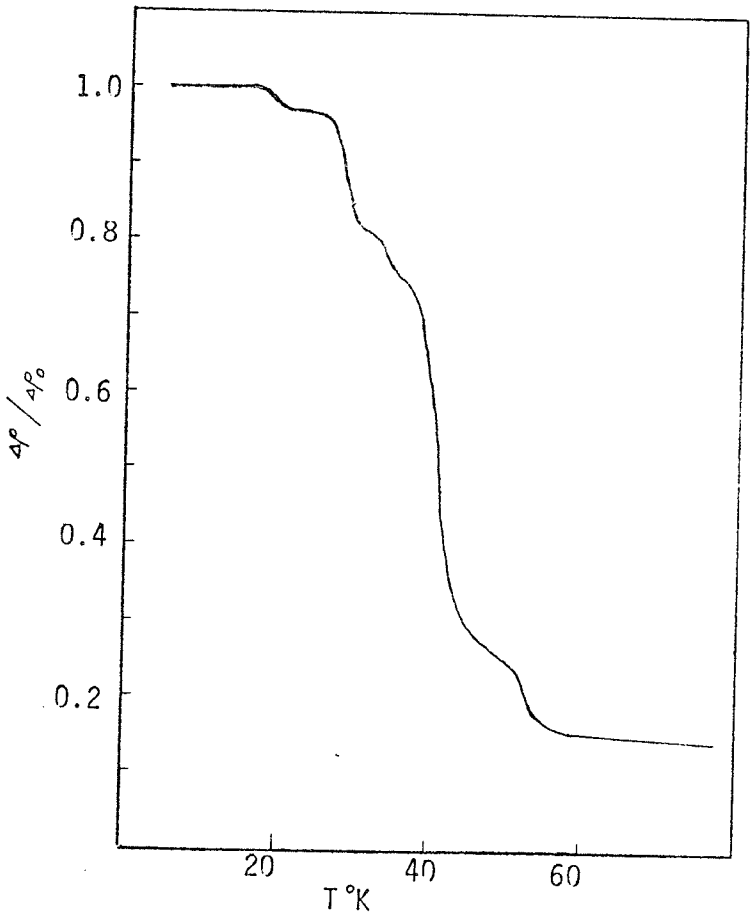

FIG. 1-2 Stage I recovery of electron irradiated copper. Data are taken from reference 38.

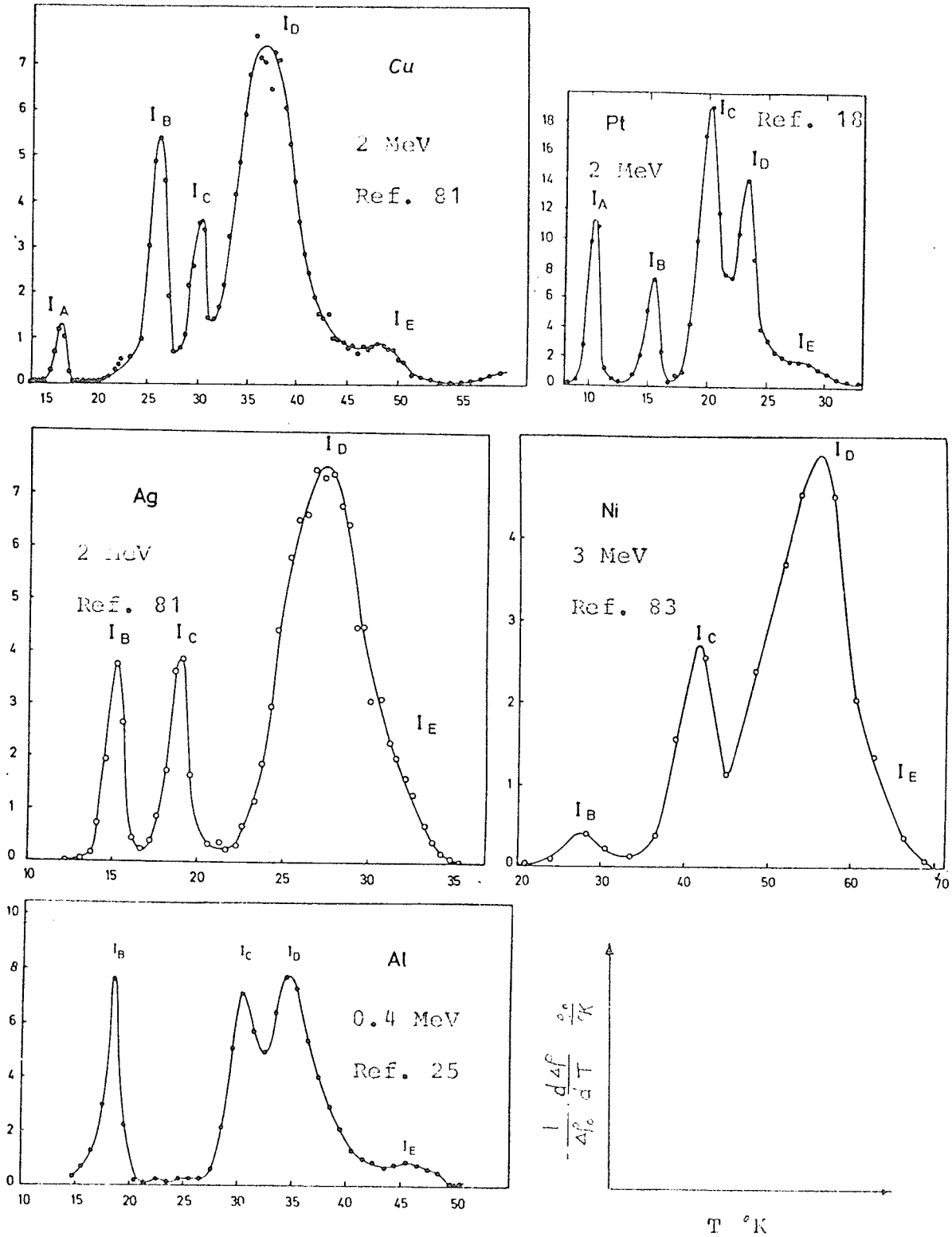

FIG. 1-3 Stage I recovery of electron irradiated metals.

$$dC/dt = \alpha C = C\nu_o \exp(-E_m/kT) = C/\tau, \qquad (1\text{-}7)$$

where τ is the life time.

(2) τ is dose independent. That is, it does not depend on the concentration of the Frenkel pairs[38, 39, 40, 81].

(3) The temperatures and the recovery rates of these substages are not changed by the quenched-in vacancies[18] and cold-work produced defects[39, 41]. (2) and (3) indicate that the interaction between the interstitial and the vacancy in a bound Frenkel pair is so strong that the other defects can not affect the migration of an interstitial to its own vacancy.

(4) The amount of recovery of the three substages depends sensitively on the energy of the incident electrons[83]. The recovery of Ib and Ic reaches a maximum when the electron energy is slightly above the threshold energy. This is expected because the lower incident energy produces more close interstitial-vacancy pairs. However the recovery of stage Ia increases slightly with increasing electron energy. There is no explanation for this abnormality.

The experimental facts mentioned above lead to the general agreement of the interpretation for Ia, Ib, and Ic. As the annealing temperature is increased, more defects are mobile and the reactions become more complex.

Stage Id and Ie are attributed to the free migration of interstitials based on the following facts.

(1) Id and Ie have the same activation energy[38].

(2) The quenched-in vacancies enhance the recovery of Id and Ie, and Ie is shifted toward Id[18, 39]. The difference between Id and Ie is that the Id interstitials require less jumps to meet the vacancies. The quenched-in vacancies reduce the mean number of jumps required by the Ie interstitials and Ie is shifted to lower temperatures.

There are two different opinions about the atomic configurations of interstitials in FCC metals.

(1) One-interstitial model (Corbett, Smith and Walker[38]). Only one type of interstitials exist in FCC metals. However, this group of authors did not specify the atomic configuration of their interstitials.

(2) Two-interstitial model (Meechan, Sosin, Brinkman[41], and the Stuttgart group).

A body-centered or type A interstitial (Fig. 1-4a) is metastable. Its energy can be lowered by sharing the lattice site with one of its nearest neighbours (Fig. 1-4b). These authors

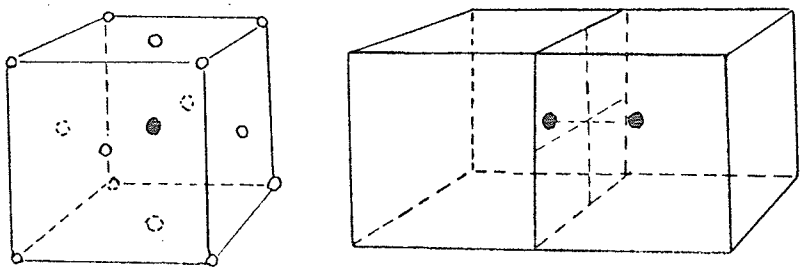

(a) (b)

FIG. 1-4 Atomic Configurations of Interstitials in the FCC Structure. (a) Type-A Interstitial; (b) Type-B or Split Interstitial.

propose that type A interstitials are mobile in stage I, and type B in stage III.

Stage II (60-220°K)

The recovery of stage II depends sensitively on the impurity in the sample and the radiation dose. The addition of impurities induces one to three substages in the stage II region depending on the impurity added. Al-0.085 at% Ga, for example, has one substage. Al-0.06 at% Mg has two substages[44]. The interpretation based on the impurity effect is that the stage II is due to the annealing out of the impurity trapped interstitials[42]. This annealing model can not explain the effect of dose dependence. In low dose irradiated pure samples, stage II is almost absent. After high dose irradiation, a continuous recovery is observed[83]. That is, the stage II is at least partly due to the intrinsic point defects. The detailed processes responsible for the stage II recovery are not yet well understood.

Stage III (220-320°K)

Several recovery models have been proposed for the stage III. The authors[38, 42] supporting the one-interstitial model suggest that stage III is due to the release of the interstitials from the deepest traps. The thermal energy in the stage II temperature range is not large enough to free these interstitials. A recent report[45] supports this interpretation. Gonser has shown

that the Mössbauer spectra of irradiated Au doped with ^{57}Co are modified after the sample is annealed in stage II. The modification is removed after annealing in stage III. He attributes this to the formation of an interstitial-impurity complex in stage II and the dissociation of the complex in stage III. A comment can be made on the impurity trapping model. If the stage III recovery is due to the impurity trapped interstitials, the activation energy would depend on the doping agent because of the difference in the interstitial-impurity binding energy. However this has not been observed[44]. In the two-interstitial model, stage III is due to the annealing out of split interstitials. The magnetic after effect experiments done by the Stuttgart group[46, 54] support this interpretation. They observed the magnetic after effect in irradiated Ni. This effect was not observed after the sample was annealed in stage III. The magnetic after effect is due to the re-orientation of the split interstitials. The vacancy model of stage III is based on the activation energy measurements in irradiated and quenched samples (Table 1-2)[47].

Table 1-2: Activation Energy of Stage III

	E_{III} (irradiated) eV	E_{III} (quenched) eV
Cu	0.69 ± 0.05	0.70 ± 0.15
Ag	0.67 ± 0.04	0.57 ± 0.03
Au	0.76 ± 0.10	0.70 + 0.05
Pt	1.36 ± 0.08	1.33 ± 0.08
Al	0.59 ± 0.04	0.57 ± 0.10
Ni	1.02 ± 0.03	0.85 ± 0.15

Although the activation energies in irradiated metals agree fairly well with the activation energies in quenched samples measured in the stage III range, the vacancy model is not without problems. As mentioned previously, quenching produces vacancies as well as vacancy clusters. The activation energy varies with the size of the cluster. The activation energy measured in the quenched sample should be considered as an effective value.

Stage IV (320-450^{o}K)

This is a small annealing stage prior to the recrystallization. It is generally ascribed to the annealing out of vacancies.

The interpretation of the point defect reactions in each stage is still in great controversy. The ambiguity of interpreting the annealing stages arises from several factors:

(1) there is still lack of systematic experimental data;

(2) an annealing stage may not be a singly activated process; and

(3) the conventional experimental techniques such as stored-energy and resistivity measurements are unable to resolve the defect species.

1.2. PRODUCTION OF POINT DEFECTS BY PLASTIC DEFORMATION

In 1952, Seitz[48] pointed out that moving dislocations could generate non-equilibrium point defects. Since then many models have been proposed to account for the production of point defects by plastic deformation. In fact, all these models

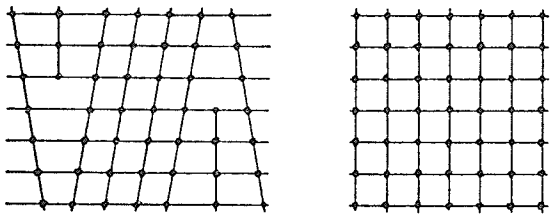

(a) a perfect crystal.

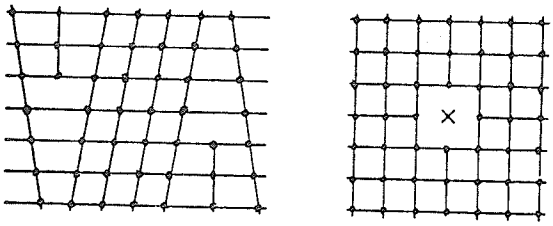

(b) a row of vacancies.

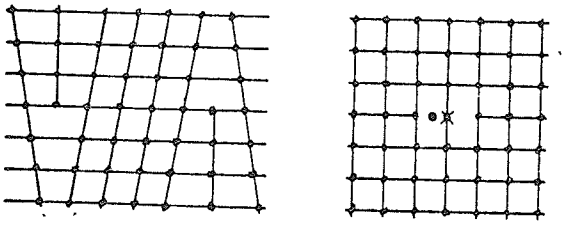

(c) a row of interstitials.

FIG. 1-5 Annihilation of positive and negative dislocations.

are based on the geometrical model of edge dislocations. Fig. (1-5a) shows a positive and a negative edge dislocation moving on adjacent planes in a simple cubic lattice. When their extra half-planes join together, the crystal becomes defect free. However, if the slip planes of the two dislocations are separated by two atomic distances (Fig. 1-5b), a row of vacancies perpendicular to the page is formed. If they glide on the same plane (Fig. 1-5c) a row of interstitials is formed. If the direction of motion of an edge dislocation is not parallel to its slip plane, a void or some extra material will be left behind. This kind of motion is called non-conservative and is diffusion controlled.

In general, only the elementary edge jogs on screw dislocations are considered to produce point defects (Fig. 1-6). The mechanisms of point defect production can be divided into two categories.

(A) Non-conservative motion of jogs

(i) Seeger's model[49]

The jog will glide along the screw dislocation, and occasionally, under thermal activation, make non-conservative jumps to generate isolated point defects (Fig. 1-6).

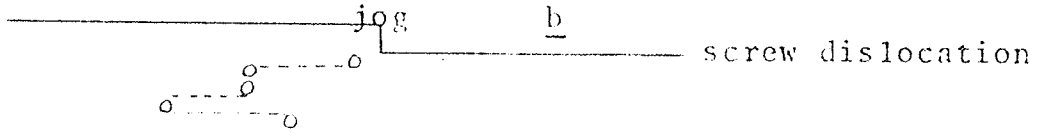

FIG. 1-6 Creation of Point Defects by non-conservative Motion of the Edge Jog on a Screw Dislocation. The dashed lines indicate the conservative motion of the jog[19].

The circles represent the point defects, and the dashed lines indicate the glide of the jog. The concentration of point defect depends on the temperature of deformation and the jog density.

(ii) Kuhlmann-Wilsodrf's "uncertainty of dislocation axis" model

According to this model, a dislocation axis is not well defined due to the thermal vibration of atoms. A segment of a screw dislocation can be transferred momentarily to a nearby plane and a pair of jogs are formed. When the dislocation moves, the jogs make non-conservative jumps and produce point defects. Based on this model, the concentration of point defect depends on temperature and is proportional to the dislocation density. Since the rate of generation of dislocations is fast in the early stage of deformation, one would expect the production of point defects to follow this trend. This is not observed experimentally. A comparison with the experimental data is shown in Chapter 3.

(B) Annihilation of Dipole Dislocations

(i) Van Bueren considers that jogs move only non-conservatively leaving behind them rows of point defects. Since a row of point defects and a dipole dislocation (Fig. 1-5b and c) are physically the same entity, it is equivalent to saying that the jog is sessile and it pulls a long dipole when the screw dislocation moves forward (Fig. 1-7).

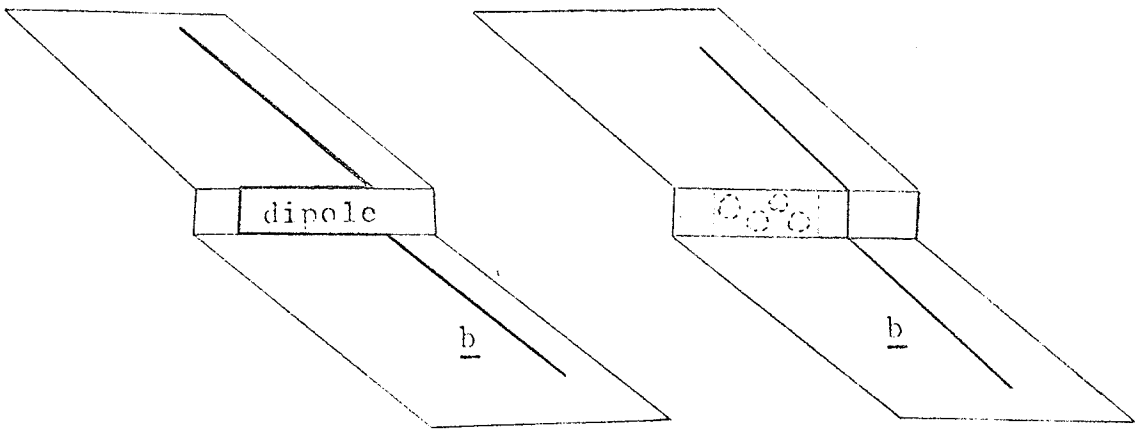

FIG. 1-7 Annihilation of Dipole Dislocation.

The generation of point defects is completed when the dipole pinches off and forms point defect clusters. A dipole can also be formed by two dislocation segments. The dislocations moving on the neighboring slip planes, for instance, can attract each other and form a dipole. The dipole mechanism has been observed by Price[64] in deformed cadmium.

(ii) Saada's Model

Friedel[78] argues that the jogs should glide easily along the dislocation to the part having edge character rather than produce point defects. The point defects are produced each time a mobile dislocation loop cuts through an attractive tree of the dislocation forest. Saada[50] derived a quantitative equation of

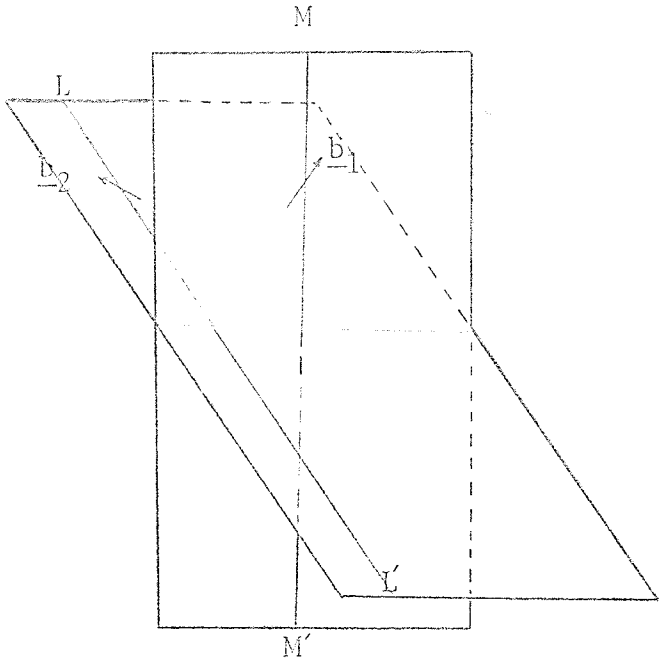

(a)

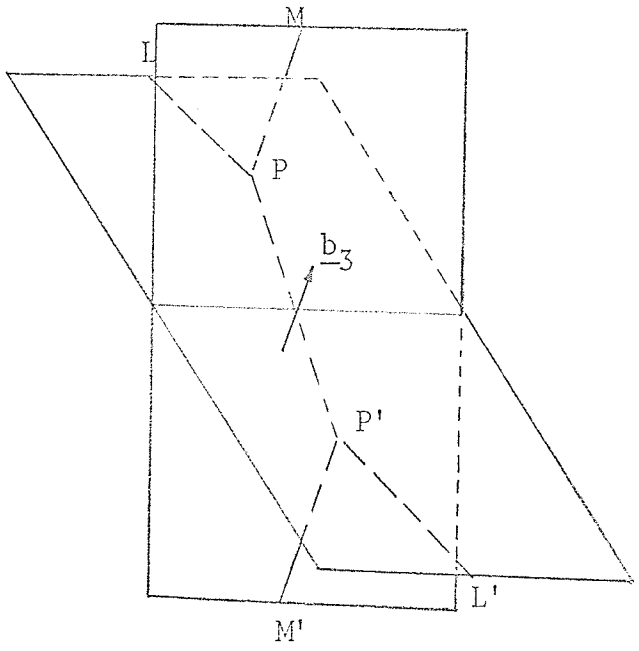

(b)

FIG. 1-8 Dislocation reaction.

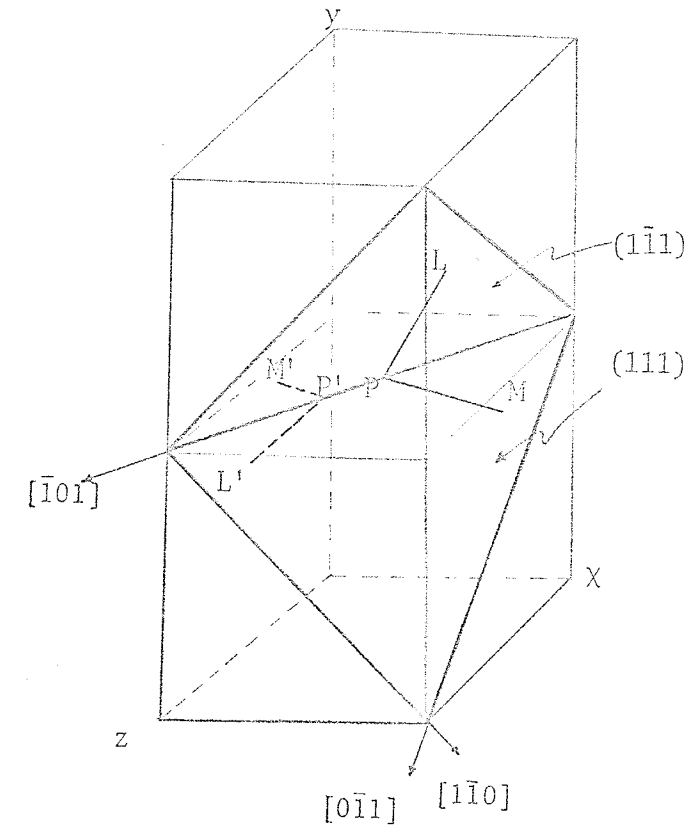

(a)

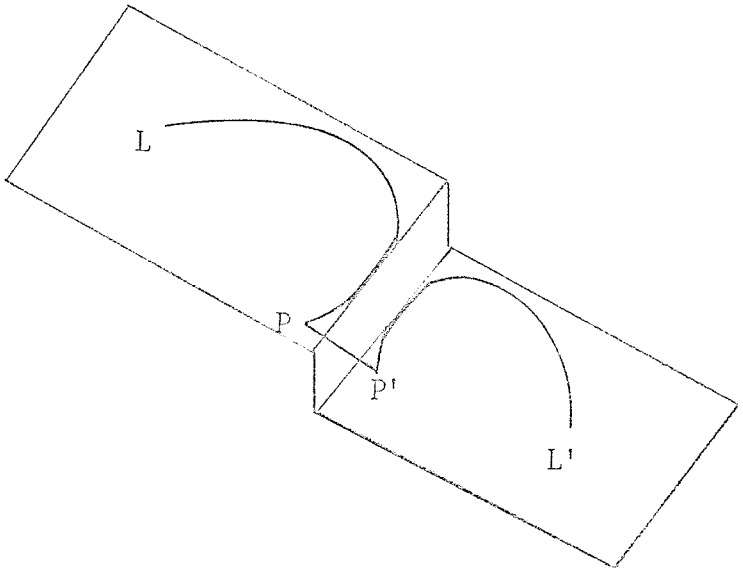

FIG. 1-9 (a) Dislocation reaction in cubic crystals.

(b) Formation of dipole dislocation.

point defect concentration based on Friedel's idea.

Consider two dislocation segments MM' and LL' (Fig. 1-8a) with Burgers vectors $\underline{b}_1$ and $\underline{b}_2$, respectively. If the force between them is attractive, the Hirsch reaction occurs when they intersect each other (Fig. 1-8b) to form an attractive junction. Since the elastic energy of a dislocation is proportional to the square of its Burgers vector. The hirsch reaction is energetically favourable if

$$b_1^2 + b_2^2 > b_3^2 \tag{1-8}$$

This is the case when $\underline{b}_1 \cdot \underline{b}_2 < 0$, (i.e. the angle between them, $\theta > \frac{\pi}{2}$). An example is shown in Fig. 1-9a. The moving loop LL' with $\underline{b}_2 = \frac{a}{2}[\bar{1}01]$ glides on $(1\bar{1}\bar{1})$ plane. The tree MM' with $\underline{b}_1 = \frac{a}{2}[1\bar{1}0]$ lies on (111) plane. They react to form a junction PP' with $\underline{b}_3 = \frac{a}{2}[\bar{1}01] + \frac{a}{2}[1\bar{1}0] = \frac{a}{2}[0\bar{1}\bar{1}]$. PP' is not mobile on $(1\bar{1}\bar{1})$ plane. However the rest segments LP and P'L' will bow out under the applied stress (Fig. 1-9b). Since $\underline{b}_1$ is not parallel to the slip plane of LL', the two segments are on different slip planes. A dipole will be formed. The length of the dipole is approximately proportional to the diameter of the loop (or the size of the dislocation network, ℓ). Thus the number of point defect produced per intersection event is $A'(\ell/b)$, where A' is a constant. The atomic fraction of point defects generated after dN attractive trees per unit volume are cut is:

$$dC = [A'(\ell/b)dN]/(1/b^3)$$
$$= A'\ell b^2 dN \qquad (1\text{-}9)$$

The corresponding increase in strain is:

$$d\varepsilon = b\ell^2 dN$$

$$\therefore \quad \frac{dC}{d\varepsilon} = A'(b/\ell) \qquad (1\text{-}10)$$

Friedel and Saada[70] point out that the cutting of the attractive trees is the dominant workhardening mechanism in FCC metals. The stress required to break the junction is:

$$\sigma \simeq \frac{\mu b}{\beta \ell}, \qquad (1\text{-}11)$$

where μ is the shear modulus, β, a constant. Combining Eq. (1-10) and (1-11) gives:

$$dC/d\varepsilon = A\sigma/\mu \qquad (1\text{-}12)$$

where $A = A'\beta$.

The total concentration of point defects produced is:

$$C = \frac{A}{\mu}\int_0^{\varepsilon}\sigma d\varepsilon \qquad (1\text{-}13)$$

That is, the concentration is proportional to the work done on the specimen during deformation.

Based on the dipole model, vacancies and interstitials are generated in approximately equal amount. The energy required to create the defects is completely supplied by the applied stress. However, in the case of the jog model, it is more difficult to drag an interstitial-producing jog than a vacancy jog because of the higher energy of formation of the interstitial. As such, one would speculate that vacancies are the dominant point defects in cold-worked metals. However, Seeger[51] argues that there should be enough energy available from the applied stress field to produce interstitials and both types of point defects are produced in approximately equal amount. There is no conclusive experiment so far. It is clear that the dislocations act as sources of point defects during plastic deformation. The reverse process occurs during annealing. That is, the dislocations are also the primary sinks for point defects. Van den Beukel[47] makes an estimate that the average number of jumps of point defects to reach a dislocation in random walk is of the order $n_j \simeq \frac{1}{\rho_d b^2}$, where ρ_d is the dislocation density and b the interatomic distance. The number of jumps to meet another point defect is 1/C. The number of jumps is smaller when the diffusion of point defects is assisted by the long range dislocation stress field. For strain between 5 and 50%, the point defect concentrations are of the order of 10^{-5} - 10^{-4}, and the dislocation densities

$\gtrsim 10^{10} - 10^{11}$ cm^{-2}. The number of jumps necessary to meet a dislocation is $n_j \simeq 10^5 - 10^4$. Therefore the average number of jumps for arriving at a dislocation is of the same order of magnitude as the number of jumps for meeting another point defect. That is the dislocations suppress the growth of point defect clusters. In quenched metals the degree of clustering is very high during annealing because of the low dislocation density.

There is strong evidence that point defects interact with dislocations before they are annihilated at the dislocations. Birnbaum[3, 12] has shown that point defects retain their identity as point defects at the dislocations and pin the dislocations. High purity copper and aluminum specimens which are deformed at 77°K, annealed at a higher temperature T_2, and then reloaded again at 77°K, show a yield point. The increase in yield stress is attributed to the pinning of dislocations by the point defects generated during deformation. There are two ways that point defects can lose their identity:

(1) they can induce climb of dislocations;

(2) they can migrate along the dislocation core (pipe diffusion) to the grain boundaries and free surfaces. The second mechanism has not been conformed experimentally.

1.2.1. Annealing Stages in Cold-Worked Metals

The point defects produced by cold-work also anneal out in four stages. There is a large annealing stage at temperatures

slightly higher than the stage IV temperature. This stage is attributed to the recovery of dislocations. The cold-worked stage I recovery is in general less than 5% of the total recoverable resistivity[55]. Comparing this with the irradiation stage I (85%), it indicates that bound Frenkel pairs are not produced by plastic deformation. This is consistent with the dislocation models which predict that point defects of the same type are generated in rows or platelets. Most of the cold-work induced point defects anneal out in stages II and III. Buck[13] has shown that the stage II recovery in cold-worked Cu single crystals is not different in 99.98 and 99.999% pure material. Schumacher and Seeger[56] and Dawson[31] even found resistivity increase in some portions of the stage II in cold-worked noble metals. This phenomenon is unexplained. In general, only one broad annealing stage is observed in the stage III temperature range for heavily cold-worked metals. However, in the present investigation, two well-defined substages occur in copper deformed at 5% strain. In cold-worked nickel Seeger et al[46, 57] observed a magnetic after effect and an internal friction peak which also annealed out in stage III. They attributed stage III to the annealing out of type B interstitials. Stage IV has not been observed in cold-worked Ag, Au, and Al. In cold-worked Cu a continuous recovery in this temperature range is observed[58, 60]. The activation energy increases continuously from 0.7 to 2 eV. Balluffi et al[59] conclude that rearrangement of dislocations plays an important part in stage IV. The study of

the annealing behaviour of point defects in cold-worked metals is still in the very early stage. The resistivity method is of limited usefulness because it can not resolve the point defect species.

1.2.2. Review of Low Temperature Plastic Deformation Experiments

The experimental investigation on point defects in cold-worked metals started with the work of Molenaar and Aarts[61]. The electrical resistivity of a copper wire was measured as a function of stress and extension at liquid air temperature (-183°C). After 8% extension the tensile deformation was interrupted to anneal the wire at room temperature. This treatment caused a decrease in the electrical resistivity, while the stress-strain curve was unaffected. The resistivity drop was ascribed to the annealing out of point defects. Druyvesteyn and Manintveld[62] performed the isochronal annealing of cold-worked copper and found that the resistivity drop occurred in two stages. Since then most investigators emphasized the study of the annealing behaviour of point defects in cold-worked metals. The quantitative description of point defects production by deformation was relatively unexplored. Since point defects and dislocations are continuously generated during plastic deformation, the quantitative measurement of point defects concentrations becomes more difficult. Fig. 1-10 shows a collection of data on resistivity increase versus strain in copper. Although there is a general agreement in the order of magnitude, the absolute

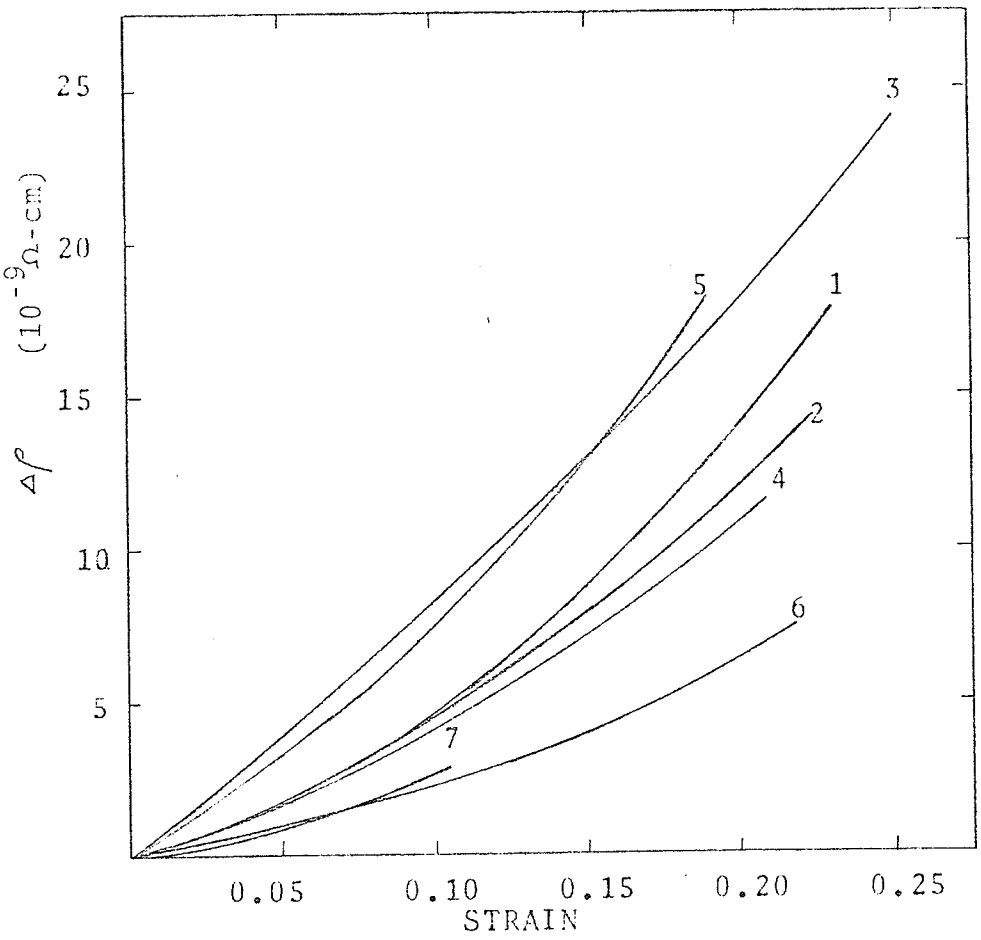

FIG. 1-10 Recoverable Resistivity vs Strain Relation

(1) Molenaar and Aarts[61], (2) Druyvestevn and Manintveld[62], (3) Berghout[43], (4) Aarts and Jarvis[74], (5) Pry and Hennig[64], (6) Jongenburger and van Bueren[86], (7) Dawson[76].

values can differ by more than a factor of 2. Most of the early investigators were unaware of the important deformation parameters such as the temperature of deformation and the strain rate. The point defect concentration C was considered as a function of strain ε alone. It was usual to fit the results to Van Bueren's empirical formula:

$$C = A\varepsilon^m, \tag{1-14}$$

where A and m were considered constants. Peiffer[66] has shown that both A and m depend on the history of deformation in copper. Since point defects are generated by dislocations, it is clear that the concentration of point defects will depend on all the deformation parameters. Hibbard[63] and Basinski and Saimoto[65] have found that the sum of the resistivities recovered due to intermittent anneals during deformation is larger than that recovered in one final anneal after an equivalent strain. Hibbard suggested that this represents a point defect saturation effect whereby more defects are removed during continuous deformation. That is, more point defects are swept away by the moving dislocation when the point defect concentration is high. Such effect of dynamic strain-ageing of point defects is difficult to control. In summary, the following conclusions may be made:

(1) The production of point defects depends on the deformation parameters.

(2) The concentration one measures at a given state of deformation represents the net amount of point defects rather than the gross amount produced.

The objectives of this work are (1) to study the dependence of point defect production on plastic strain and strain energy, (2) to investigate the effect of strain rate and temperature of deformation, and (3) to investigate the effects of impurities on the production and annealing of point defects in cold-worked copper.

2. EXPERIMENTAL TECHNIQUES

2.1. SPECIMEN PREPARATION AND METALLOGRAPHY

The materials used in the experiments were Johnson-Matthey 99.999% Cu and the commercial grade 99.98% Cu. The as received copper bar of 0.5 inch in diameter was cleaned in dilute nitric acid and methanol to remove the oxide layer. It was then sealed in a pyrex tube at a pressure better than 10^{-4} torr, and annealed at 600°C for 2 hours. The recrystallized bar was swaged to a diameter of 0.322 inches and annealed again at 600°C for 2 hours. The intermediate heat treatments were to prevent the formation of small cracks during cold rolling. The copper bar was rolled in one direction to a thickness of 0.2 mm. A group of the thin strips of 10 cm long were clamped together and cut to the size shown in Figure 2-1.

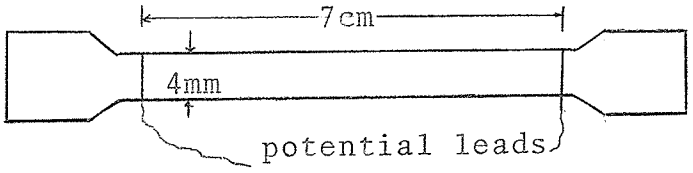

FIG. 2-1

The potential leads were copper wires of 0.2 mm in diameter spot welded at each end of the gage length. The specimens were carefully cleaned and sealed in high vacuum. The final heat treatment was at 600°C for four hours and air cooled to room temperature. It yielded an average grain size of 33 μm.

An electrolyte containing one part concentrated nitric acid and two parts methyl alcohol was used to polish both metallography and electron microscope specimens. The polishing conditions were -40°C at a potential of 5 volts. At room temperature, the same solution became a good etchant to reveal the grain boundaries.

2.2. RESISTANCE MEASUREMENT

The major instrument for the electrical resistance measurements was a Guildline 9920 Direct Current Comparator Bridge which was developed by the National Research Council of Canada.

The conventional potentiometric method involves a comparison of voltage drops when the same current passes through a specimen and a standard resistor. The ratio of the resistances $\frac{R_x}{R_s}$ is obtained from the ratio of voltage drops $\frac{e_x}{e_s}$ (Figure 2-3). The resolution and accuracy are limited by the stability of the currents in the tested resistor and in the potentiometer. An important factor which determines the temperature stability of a resistor is its power dissipation. Self-heating will increase the resistance. The potentiometric method suffers from the disadvantage that when scaling resistors in decade steps the same current must be passed through the specimen and the standard resistor, and hence more heat is generated in the larger resistance.

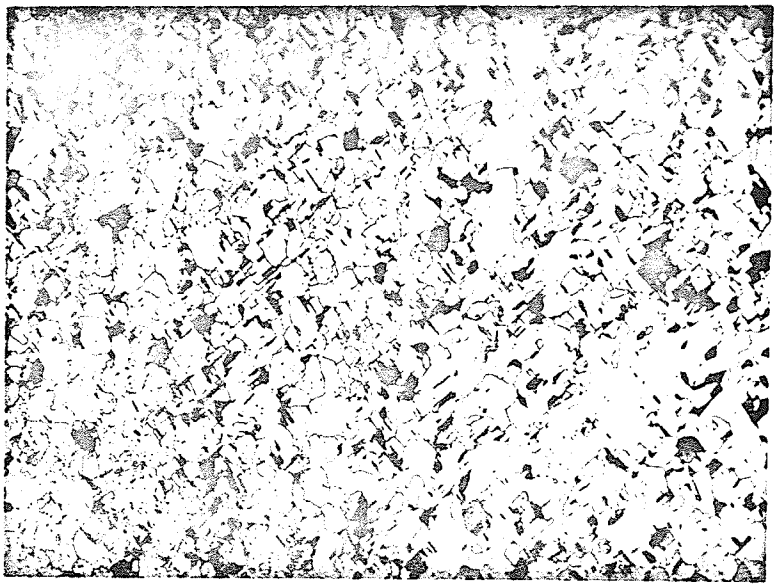

FIG. 2-2 Recrystallized Copper.

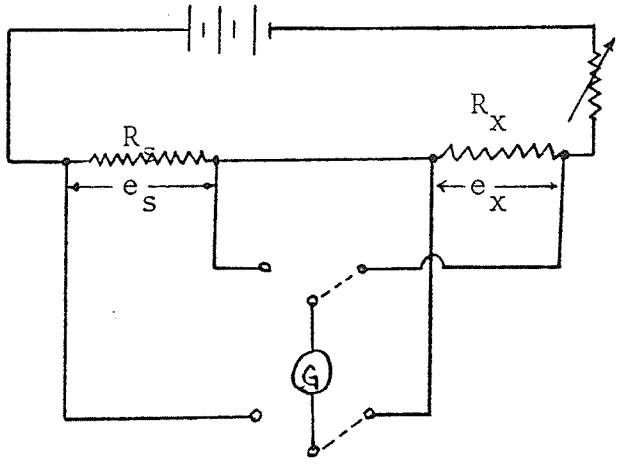

FIG. 2-3 Potentiometer Method.

2.2.1. Direct Current Comparator Bridge

The Guildline 9920 D. C. Comparator Bridge employs the principle of ampere-turn balance. The ratio of the resistances R_x/R_s is obtained from the ratio of the number of turns of the coils which can be determined with extremely high accuracy. The resolution of the bridge is 1 part in 10^7.

The bridge consists of a toroidal transformer, a galvanometer system, a magnetic flux detection system, and a power supply unit (Fig. 2-4).

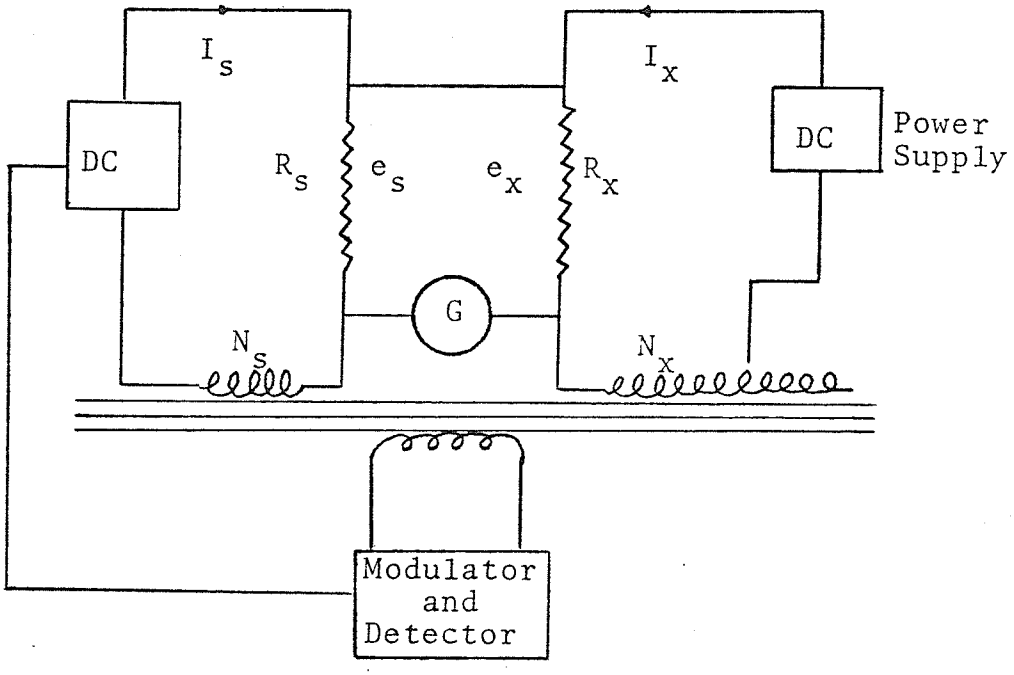

FIG. 2-4 D. C. Comparator Bridge.

The toroidal transformer has a primary N_s and secondary N_x windings which carry direct current, and modulation and detection windings which carry AC current. When the primary and secondary ampere-turns are equal and opposite, the resultant magnetic flux in the toroidal core is zero.

This condition is detected and automatically maintained by the modulation and detection units. The galvanometer system detects the voltage difference across the specimen and the standard resistor. It consists of a photocell amplifier and a secondary galvanometer. The off-balance current produced at the photocell drives the secondary galvanometer. The photocell amplifier has a sensitivity of 0.01 microvolt. With one volt across the specimen, this is equivalent to the resolution of one part in 10^8.

2.2.2. Operation of the D. C. Comparator Bridge

When the galvanometer indicates zero voltage, the voltage drops across the specimen and the standard resistor are equal.

$$e_s = e_x,$$

$$I_s R_s = I_x R_x,$$

or

$$\frac{R_x}{R_s} = \frac{I_s}{I_x} \qquad (2\text{-}1)$$

When the magnetic flux in the toroidal core is zero, we have:

$$I_s N_s = I_x N_x,$$

or

$$\frac{I_s}{I_x} = \frac{N_x}{N_s} \tag{2-2}$$

Combining Eqs. (2-1) and (2-2), we obtain:

$$\frac{R_x}{R_s} = \frac{N_x}{N_s} \tag{2-3}$$

The resistance of the specimen is:

$$R_x = \left(\frac{N_x}{N_s}\right) R_s$$

Since the ampere-turn balance is automatically maintained in the comparator bridge, only the galvanometer balance has to be achieved in the actual operation. At the balanced conditions, the power consumed in the resistors are:

$$P_s = \frac{e_s^2}{R_s}, \text{ and } P_x = \frac{e_x^2}{R_x}$$

$$\therefore \quad \frac{P_x}{P_s} = \frac{R_s}{R_x} \tag{2-4}$$

That is, more power is consumed in the resistor which has smaller resistance value. Since all the specimens used in the experiments

are thin, and they are immersed in liquid nitrogen, the error due to self-heating is unimportant.

The procedures of operation are as follows:

(1) Connect a specimen and a standard resistor to the proper terminals at the back of the bridge. R_S should be close to R_X.
(2) Set the secondary galvanometer sensitivity to 1/1000 and adjust the mechanical balance to bring the light spot to the center of the scale. Then set the sensitivity to 1/1 and re-zero the light spot by adjusting the zero control on the photocell amplifier.
(3) Set an approximate value of R_X/R_S on the dials. Turn the two clock-dial controls to obtain the required currents I_X and I_S. Operate the reversing switch and, at the same time, adjust I_S to obtain a null indication on the comparator balance meter.
(4) Adjust R_X/R_S dials to obtain the same galvanometer deflection in both current polarities. Then the (R_X/R_S) value shown on the dial multiplied by the standard resistance is the specimen resistance.

2.2.3. Compensation for the Temperature Fluctuation in the Liquid Nitrogen Bath

All the electrical resistances were measured at $78^{\circ}K$ by immersing the specimens in a liquid nitrogen bath. However, the boiling point of liquid nitrogen changed from time to time due to the variation in the barometric pressure. An annealed specimen

used as a dummy was always put beside the deformed specimen to detect the change in resistance due to the temperature fluctuation. The correction was done under the assumption that the same percentage change in resistance occurred in the dummy as well as the deformed specimen whenever there was a temperature change. All the lead wires were insulated and weaved together to reduce the spurious emf.

2.3. ANNEALING METHODS

2.3.1. Isothermal Annealing

The isothermal annealing method is used to measure the concentration of point defects produced after deformation. The resistivity ρ_1 (Fig. 2-6) of the specimen immediately after the tensile deformation is measured. Then it is sealed in a pyrex tube in a vacuum better than 10^{-4} torr and heated in a constant temperature oil bath at $170^{\circ}C$ for four hours. The decrease in resistivity, $\Delta\rho = \rho_1 - \rho_2$, is proportional to the point defects concentration. The temperature at the end of the stage IV^{60} is

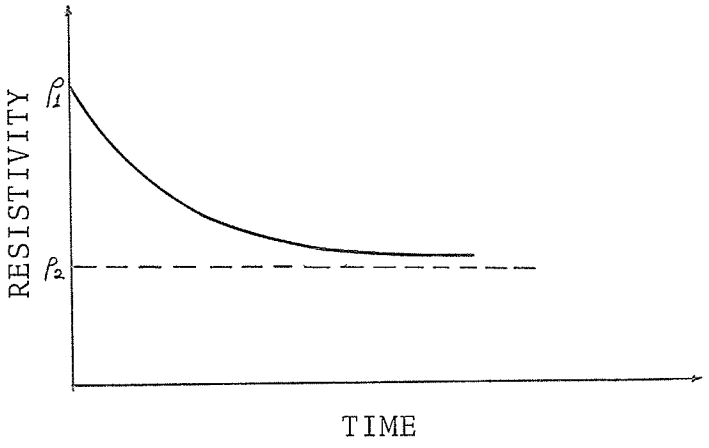

FIG. 2-6 Isothermal Annealing.

chosen as the isothermal annealing temperature.

2.3.2. Isochronal Annealing

The isochronal annealing is carried out in five-minute-10°C steps. This is approximately equivalent to a constant heating rate of 2 degrees per minute. After deformation in a liquid nitrogen bath, the specimen is warmed up step by step at equally spaced temperatures. At each temperature the specimen is kept for a fixed interval of time. At the end of each annealing step the resistivity of the specimen at the liquid nitrogen temperature is measured. The plot of the resistivity ρ versus the annealing temperature T is called an isochronal (Fig. 2-7).

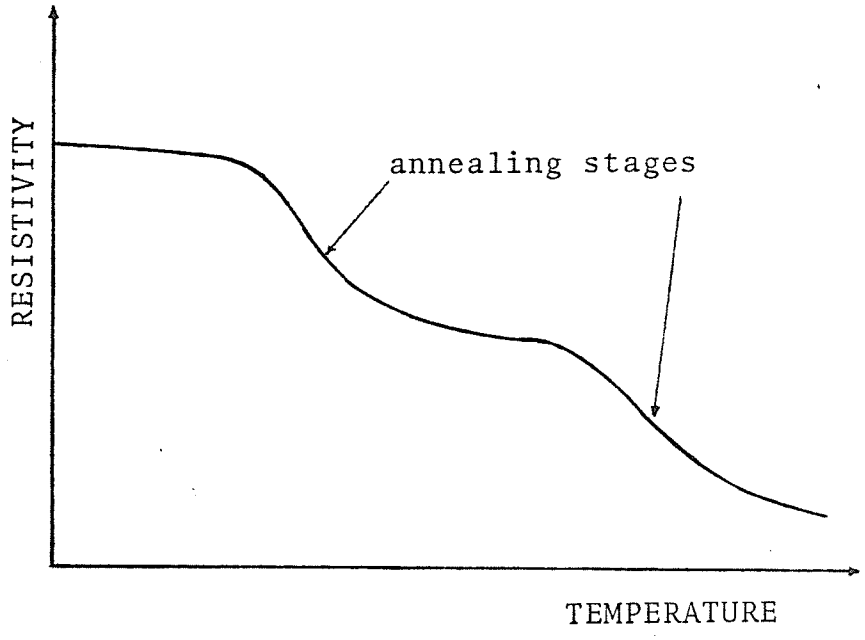

FIG. 2-7 Isochronal Annealing.

Whenever a particular group of defects anneal out, a step appears on the isochronal. In other words, an isochronal reveals the migration characteristics of different defect species. The annealing temperatures between -70°C to room temperature are obtained in a glass dewar filled with acetone and dry ice mixture. From room temperature to 80°C, a water bath equipped with a constant temperature circulator is used. The annealing at temperatures higher than 80°C are done in an oil bath.

3. RESULTS AND INTERPRETATIONS

3.1. RESISTIVITY OF METALS

The resistivity of a non-magnetic metal arises from the scattering of the conduction electrons by lattice phonons and crystal imperfections such as impurities and structural defects. The phonon contribution to the resistivity approaches zero when the temperature approaches the absolute zero. The residual resistivity then is a direct measure of the crystal imperfections. Matthiessen's rule states that the resistivity due to crystal imperfections is independent of temperature. Thus the total resistivity is given by:

$$\rho_{total} = \rho_{ph}\ (T) + \rho_o, \qquad (3\text{-}1)$$

where $\rho_{ph}\ (T)$ is the resistivity of the defect free crystal at temperature T, and ρ_o, the resistivity due to crystal imperfections,

that is the resistivity at the absolute zero temperature.

For the non-interacting defects such as single vacancies and interstitials, it is reasonable to assume that the corresponding residual resistivity is directly proportional to the defect concentration.

Let the concentration of a particular type of defect change from C(1) to C(2) while keeping the population of the other types of defects constant. Then,

$$\Delta C = C(2) - C(1) \tag{3-2}$$

and the corresponding change in residual resistivity is:

$$\Delta\rho_o = \rho_o(2) - \rho_o(1)$$

$$= \rho_{total}(2) - \rho_{total}(1) \tag{3-3}$$

$$\Delta\rho_o = \text{const.} \times \Delta C \tag{3-4}$$

That is, the variation of the residual resistivity due to this type of defect is simply the change of the total resistivity if one measures the resistivities at a fixed temperature.

Since an interstitial produces a larger lattice strain than that of a vacancy, an interstitial contributes more resistivity[67]. Let ρ_I and ρ_V be the resistivities due to unit

concentration of interstitials and vacancies, respectively. Eq. (3-4) may be written as:

$$\Delta\rho_o = \rho_I \cdot \Delta C_I + \rho_V \cdot \Delta C_V$$

Assuming vacancies and interstitials are produced in approximately equal amount, $C_I \simeq C_V = C$, after complete annealing $\Delta\rho_o$ is still proportional to the point defect concentration produced by deformation,

$$\Delta\rho_o = (\rho_I + \rho_V)C$$

If $C_V \neq C_I$, then $\Delta\rho_o$ does not give an absolute measure of the defect concentration.

Deviations from Matthiessen's rule have been found experimentally by Dugdale and Basindki[69] for impurity defects. They define the deviation Δ by:

$$\Delta = \rho_{total} - (\rho_{ph} + \rho_o) \qquad (3\text{-}5)$$

The deviation varieswith the impurity concentration and temperature. It reaches a maximum at 70^oK in Cu-dilute Ge alloys (Fig. 3-1).

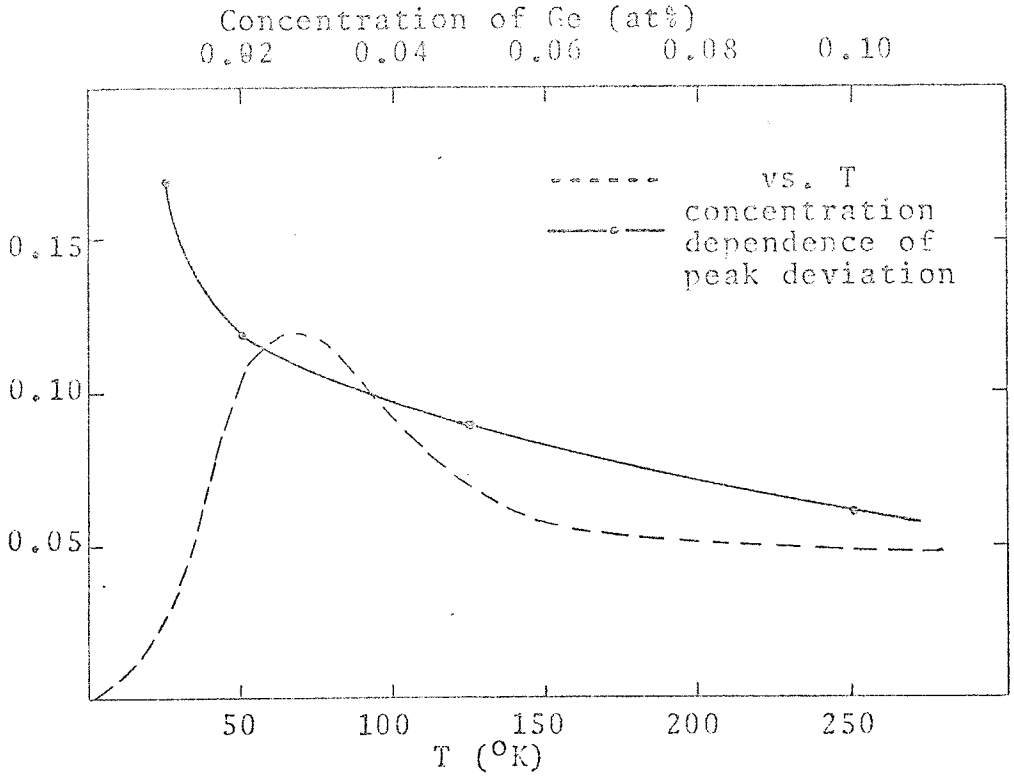

FIG. 3-1 Deviation from Matthiessen's Rule for Copper Dilute Ge Alloys. Data are taken from reference 69.

Rösch et al[68] also found the departure from Matthiessen's rule for point defects produced by cold-work in platinum (Fig. 3-2). The deviation is not so severe as that due to impurities. Their isochronal curves measured at 42°K and 77°K are not in coincidence. Fortunately, the differences are within 3% of the total recoverable resistivity. We thus assume that the deviation due to the structural point defects in copper is also small.

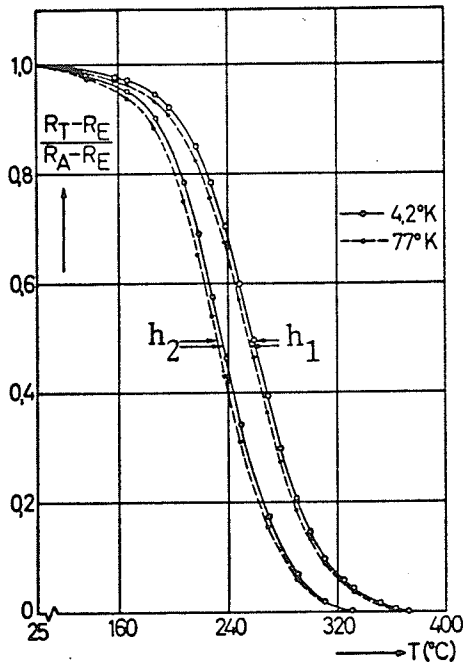

heating rate

h_1 = $10^{\circ}C/5$ min.

h_2 = $10^{\circ}C/20$ min.

R_A = resistance before anneal.

R_E = resistance after anneal.

R_T = resistance after anneal at temp. T

FIG. 3-2 Isochronal Annealing of Deformed Pt.[68]

3.2. VARIABLES CONTROLLING POINT DEFECTS PRODUCTION

During plastic deformation one is dealing with 10^6 - 10^{10} lines/cm^2 of dislocations. This is a many-body problem. To solve the motion of each dislocation line is impossible. However, the macroscopic behaviour of metals such as stress-strain relation and average amount of point defect production can be predicted under properly controlled conditions. In general, any variable, which affects the dislocation motion, will change the point defect production. The important variables are considered below.

3.2.1. The Plastic Strain and Strain Energy

The plastic strain is the most important parameter of point defect production by deformation. This is the reason that most of the previous data are fitted to Van Bueren's formula (Eq. 1-14):

$$C = A\varepsilon^m,$$

where A and m are considered as constants for a given metal and grain size. To determine the increase in point defect concentration with the plastic strain, four completely recrystallized specimens of average grain diameter of 33 μm were deformed in a liquid nitrogen bath on the Instron tensile testing machine. The resistance after the deformation R was measured at 77°K. Then the specimens were heat treated at 170°C for four hours and their final resistances R' were measured again at 77°K. The resistance increase due to point defect is $\Delta R = R - R'$. The precision of the absolute resistivity ρ is limited by the uniformity of the specimen cross-section and the accuracy in the measurement of the shape factor A/ℓ (cross-section/distance between the potential leads). Only the resistivity ratios, $\frac{\Delta\rho}{\rho} = \frac{\Delta R}{R}$, are used in the plots to eliminate the error introduced by the shape factor. The results are shown in Fig. (3-3) and Table (3-1). The concentration of point defects increases lineally with strain for $\varepsilon > 2.5\%$. In the lower strain region (<2.5%) the rate of resistivity increase is rather slow although the exponent m is apparently greater than 1.

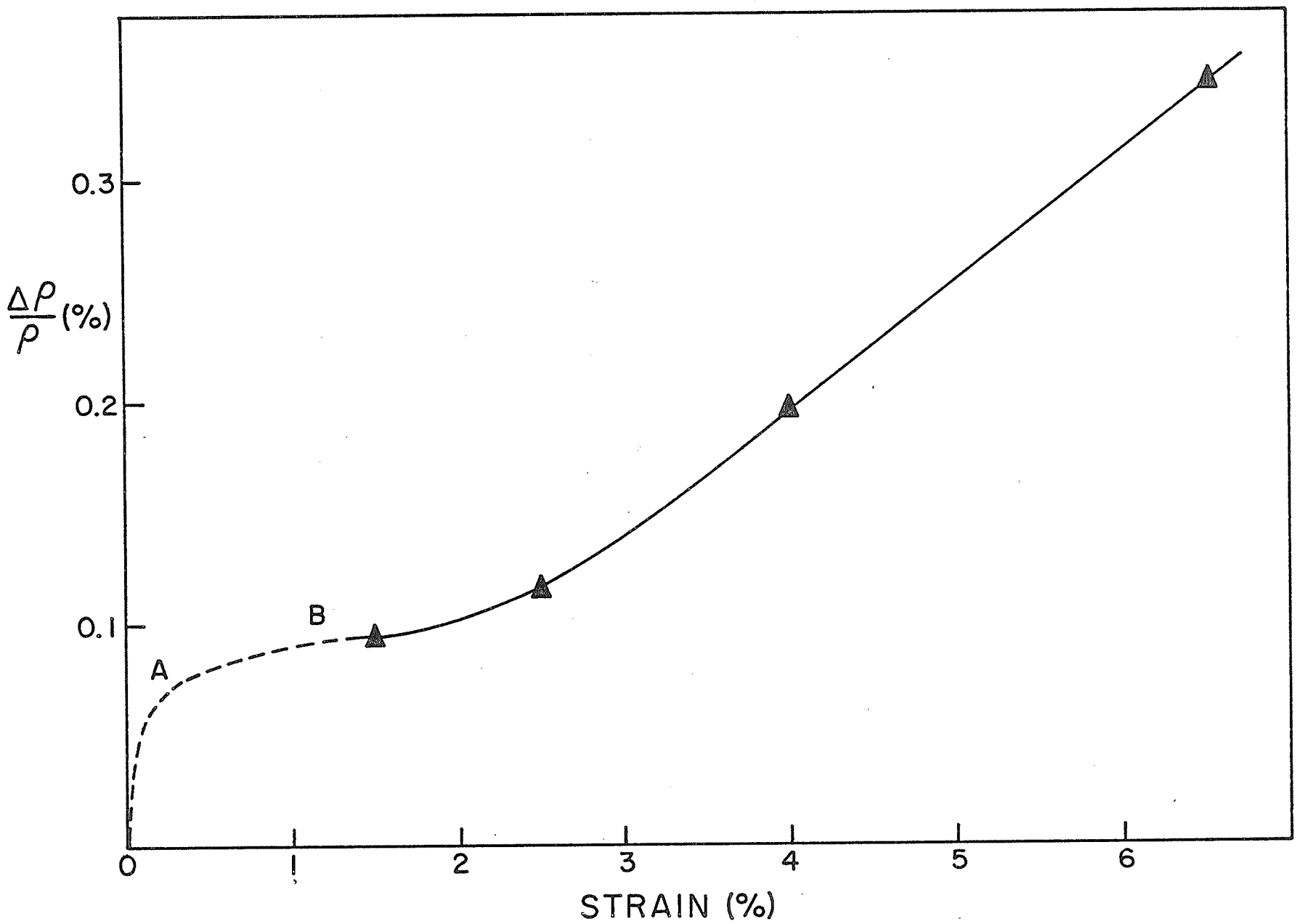

FIG. 3-3 Recoverable Resistivity vs. Strain.

Table 3-1 Recoverable Resistivities.

Grain Diameter = 33 μm
Strain Rate = 2×10^{-5} sec.$^{-1}$
Temperature = 78^{o}K

Specimen No.	Stress (Kg/mm^2)	Strain %	Strain Energy (Kg/mm^2)	R/R %
20	13.76	6.53	5.80	0.344
21	12.53	4.00	3.43	0.192
22	9.10	2.50	1.65	0.117
23	7.06	1.50	0.77	0.095

$\Delta R/R = \Delta\rho/\rho$
ΔR = resistance due to point defects.
R = resistance after deformation.

The curve does not intersect at the origin if it is extrapolated to the zero strain. This strongly indicates that the rate of point defect generation must be high in the very early stage of deformation. Singh[84] has investigated the point defect production near the pre-macroyield region in polycrystalline nickel. His results show that the point defect production rate is extremely high for strains less than 0.05%. This is simulated here by the dashed line in Fig. (3-3). Therefore, the point defect production by tensile deformation may be divided into three stages. Stage A is the pre-macroyield region. In this stage, the dislocations glide on the slip planes which have the highest resolved shear stress (i.e. easy glide). The only powerful mechanism for generation of point defects is the dipole mechanism, because the jog density and the probability of cutting trees of the dislocation forest are still low during this stage of deformation. As pointed out by Friedel[70], two dislocation loops L_1 and L_2 (Fig. 3-5) of opposite Burgers vectors $\underline{b}_1 = -\underline{b}_2$ moving on the neighbouring slip planes will have long range attractive interaction. When they move close to each other, a long dipole will be formed. The pinching of the dipole at both ends results in the creation of a row of point defects and two jogs J_1 and J_2. The dipole can break up into small loops. Such loops are considered here as point defects aggregates based on the geometrical model of edge dislocation mentioned in section 1.2. An edge dipole and a row (or sheet) of point defects correspond to the same atomic arrange-

ments. The small loops can be seen by transmission electron microscope. A copper specimen was deformed at 78°K to 10% strain. The thin foil was made immediately after deformation. The micrograph is shown in Fig. (3-4). The loops, giving rise to a half-moon contrast, are pointed out by the arrows in the micrograph.

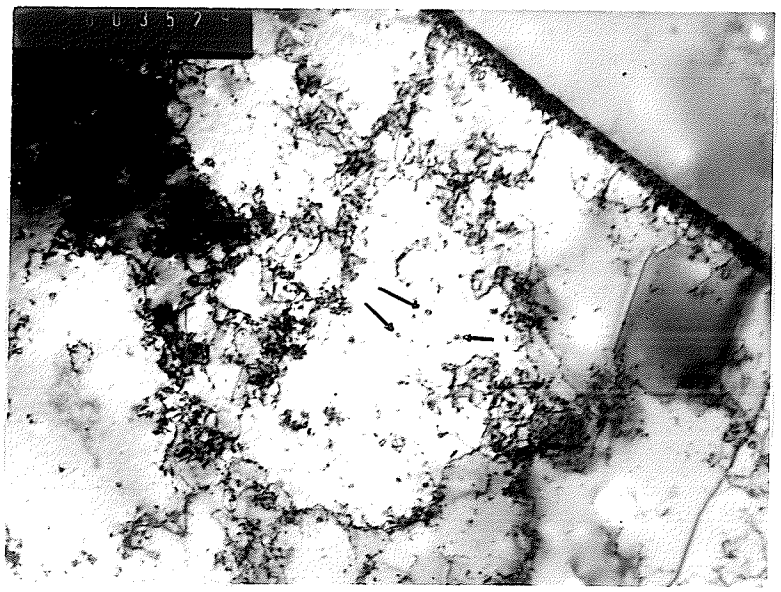

FIG. 3-4 Electron Micrograph of Deformed Copper. (×31,000)

The annihilation of the dipole dislocation is instantaneous[78] if the attractive force between the dislocations is greater than the force of climb. The force per unit length of dislocation F_c required for the climb is given by:

$$F_c \cdot b = E_f \cdot \frac{b^2 \sin\psi}{b^3}$$

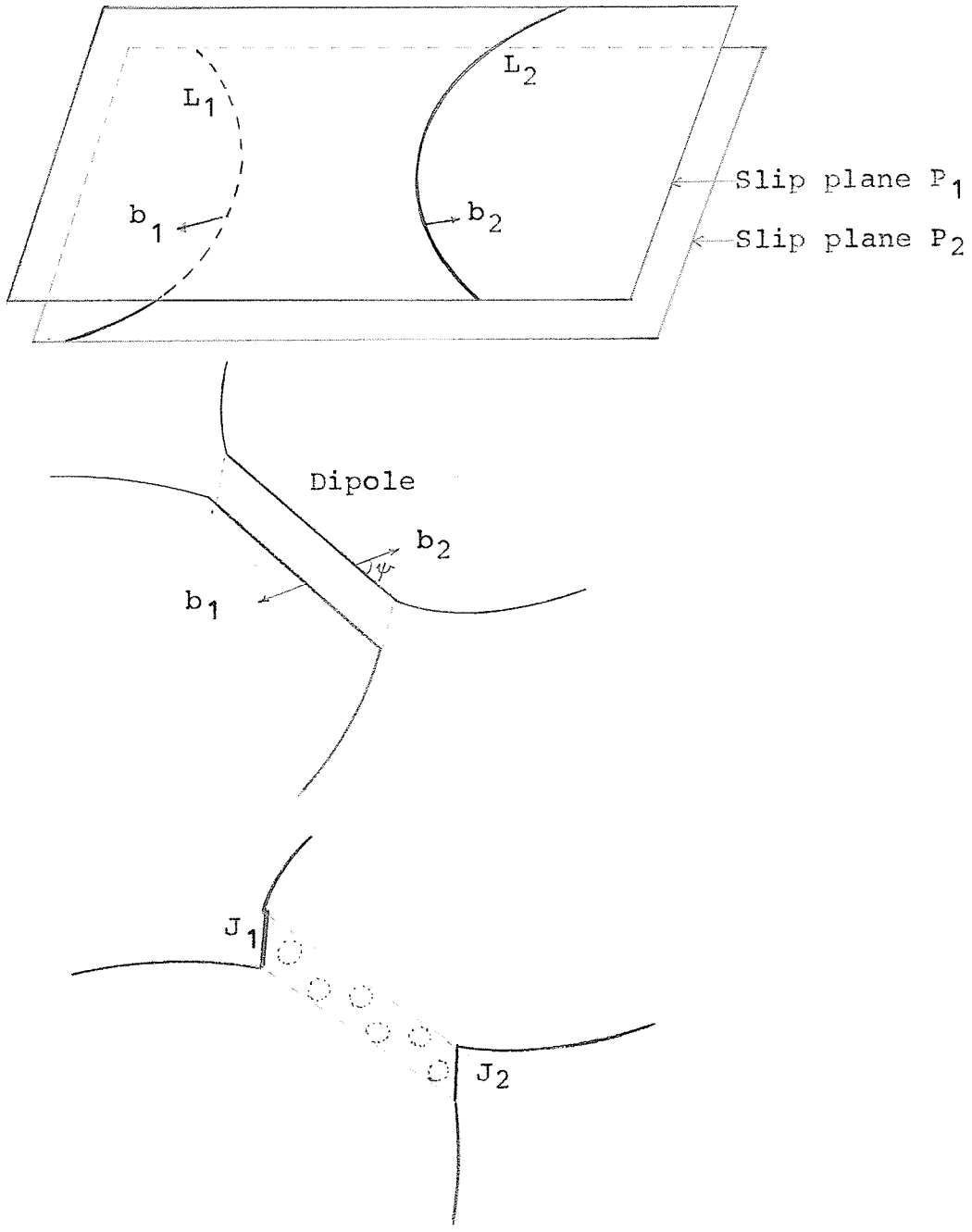

FIG. 3-5 Annihilation of dipole dislocation.

$$F_c = \frac{E_f}{b^2} \sin\psi, \tag{3-6}$$

where E_f is the energy of formation of a point defect, ψ, the angle between the dislocation line and its Burgers vector. The attractive force between two parallel dislocations is:

$$F_a = \frac{\mu b^2}{2\pi K\gamma}, \tag{3-7}$$

where K varies between 1 and (1-$\hat{v}$) and γ the distance between the dislocations. For climb to occur,

$$F_a \geq F_c,$$

$$\frac{\mu b^3}{2\pi K E_f \sin\psi} \geq \frac{\gamma}{b} \tag{3-8}$$

E_f is of the order of $\frac{\mu b^3}{5}$, the Poisson's ratio $\nu \leq 0.4$. Eq. (3-8) is valid if the dipole dislocations lie on the neighbouring slip planes.

The length of the point defects "string" formed by the annihilation of a dipole is of the order of the length of the dislocation loop. This is responsible for the high rate of generation of point defects in the microyield region. However the dipole mechanism is soon exhausted, because the obstacles such as grain boundaries are encountered by the moving dislocations. The piled-up groups and tangles of dislocations start to form

beyond the strain of 4×10^{-4} in polycrystalline nickel[84]. The defect production rate slows down in stage B (Fig. 3-3). Apparently, no appreciable amount of point defects is produced in this stage. As the applied stress increases, several (111) type of slip planes become operative. A moving dislocation has to cut through the trees threading the slip plane. Saada's mechanism is probably the dominant one in stage C. To compare with Saada's model, the recoverable resistivity is plotted versus the strain energy shown in Fig. (3-6). The strain energy, which is the work done by the applied stress, is obtained by measuring the area under the stress-strain curve using a planimeter. Saada's model predicts that the concentration of point defects produced by cold-work is proportional to the strain energy (Eq. 1-13),

$$C = \frac{A}{\mu} \int_0^{\varepsilon} \sigma d\varepsilon \qquad (3\text{-}9)$$

That is, C vs. $\int_0^{\varepsilon} \sigma d\varepsilon$ plot is a straight line. Fig. (3-6) shows that the rate of point defect production is definitely faster than Saada's prediction. This is in agreement with the results of Basinski and Saimoto[65]. However, Kapicka and Polak[71] in their recent report claim that their data fit Saada's formula. They anneal the deformed polycrystalline copper specimens at 100°C for 10 minutes. Dawson[60] has done a systematic isochronal annealing experiment for cold-worked copper. His results indicate that stage IV is centered at 150°C with 5-minute-10-degree heating rate.

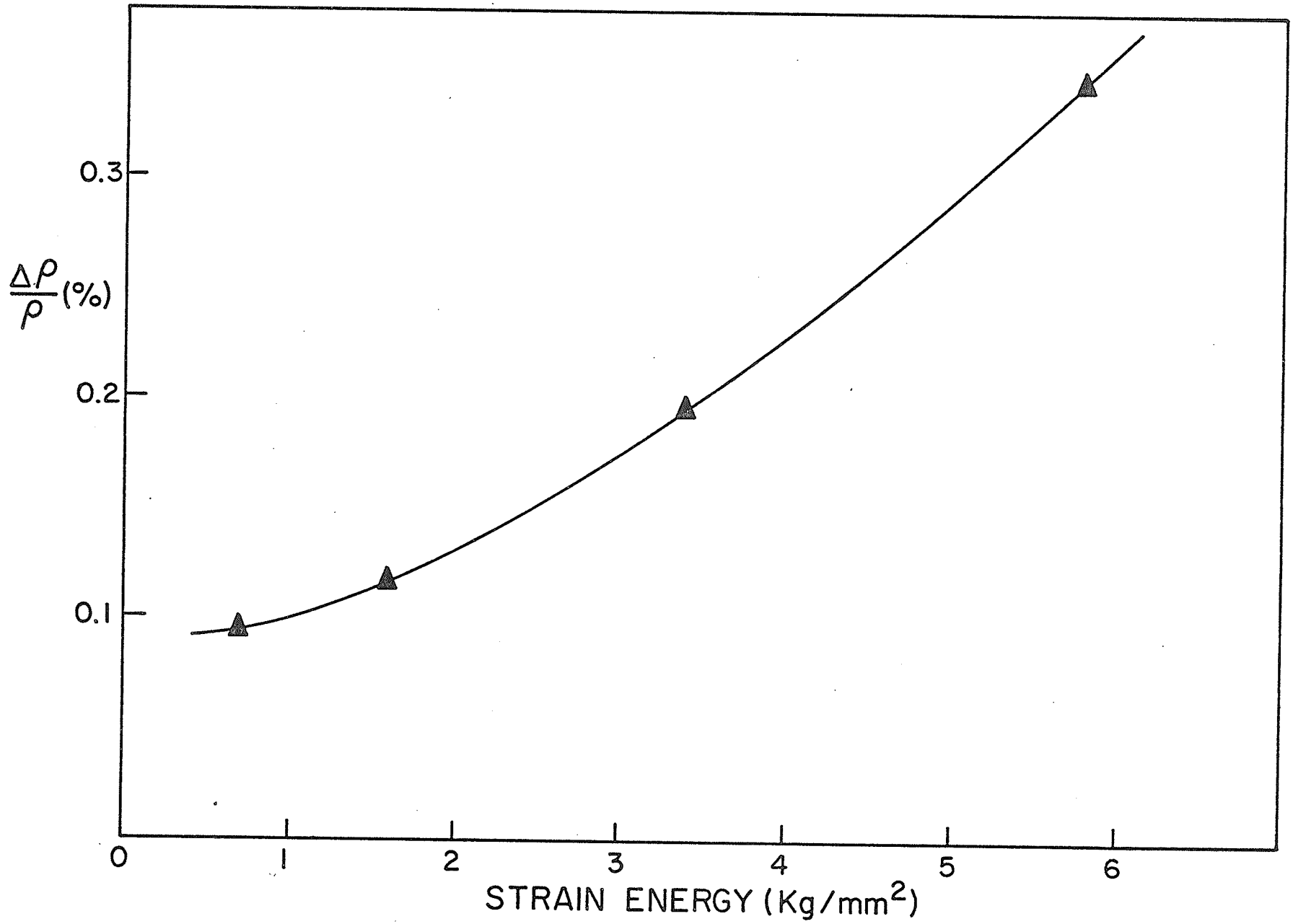

FIG. 3-6 Recoverable Resistivity vs. Strain Energy.

Based on Dawson's results, Kapicka and Polak's annealing temperature is too low and the annealing time is too short. This is why their resistivity-strain energy data fall on a straight line.

There are two possible explanations for the fast rate of point defect generation in stage C (Fig. 3-3 and 3-6).

(1) Assume the cutting of the attractive trees is the dominant mechanism. Then, there must be a flaw in Saada's formula. In deriving Eq. (3-9), Saada makes the assumption that the number of point defects produced each time a moving loop cuts an attractive tree is proportional to the size of the dislocation network according to the relation:

$$x = A'\ell, \tag{3-10}$$

where x is the length of the point defect string, A' a constant, and ℓ the average size of the dislocation network. The number of point defects produced after the moving loop sweeps a unit area is $(\frac{x}{b}) \cdot (\frac{\rho_d}{2})$, where ρ_d is the forest dislocation density assuming half of the trees are attractive. Since ρ_d varies with $1/\ell^2$, the concentration should increase with x/ℓ^2. Assuming the validity of Eq. (3-10), Saada obtains

$$\frac{dC}{d\varepsilon} = A'(\frac{b}{\ell})$$

In view of the present result, the rate of increase should be faster than $1/\ell$. Eq. (3-10) can be obtained from Fig. (3-7a) and (1-8b).

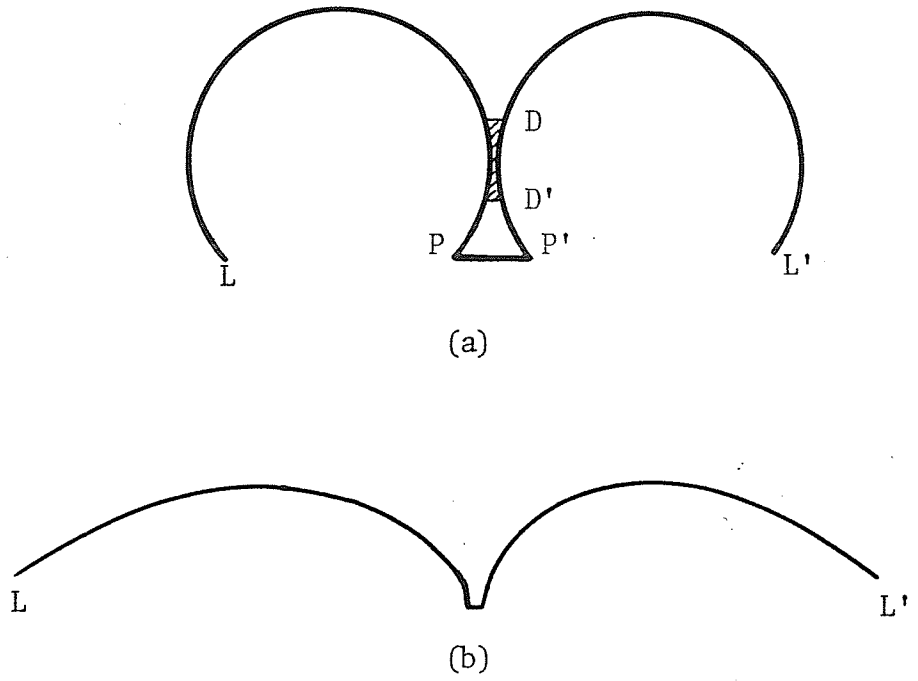

FIG. 3-7 Generation of Point Defects by Saada's Mechanism.

The length of the dipole DD' is proportional to the diameter of the loop. The configuration shown in Fig. (1-8b) is stable without

the external stress. However, under the applied stress the sessile dislocation pp' should shrink to the size of a jog before the moving loop breaks away from the tree (Fig. 1-9b). For dislocation density of 10^{10} cm^{-2}, ℓ is of the order of 10^{3}Å. The situation is represented by Fig. 3-5b. Van den Beukel[47] has estimated the magnitude of A' as of the order of 0.02. That is,

$$x \simeq 0.02\ \ell$$

Saada predicts A' = 0.2 which is one order of magnitude larger than the experimental value. Fig. (3-7b) is more realistic. A short dipole is formed and annihilated before the loops LP and L'P' bow out extensively. In this case the dipole length x is insensitive to the length of the moving loop. x depends, to certain extent, on the kinetic energy (or velocity) of the moving loops[72]. For a given strain rate,

$$x = x_o = \text{constant} \qquad (3\text{-}11)$$

Following the procedures shown in Section 1.2., we obtain:

$$\frac{dC}{d\varepsilon} = \frac{x_o b}{\ell^2} = \frac{x_o \beta^2}{\mu^2 b}\,\sigma^2, \qquad (3\text{-}12)$$

and

$$C = \frac{A''}{\mu^2 b} \int_0^{\varepsilon} \sigma^2 d\varepsilon \qquad (3\text{-}13)$$

where $A'' = x_o \beta^2$. Basinski and Saimoto[65] claim their results are in better fit with Eq. (3-13) at large deformations.

(2) The second possibility is that the production of point defects by other mechanisms such as those mentioned in Section 1.2. is not negligible. The competing mechanism will be discussed in the following section.

3.2.2. The Effect of Strain Rate and Temperature of Deformation

Takamura[88] et al have found the concentration of point defects produced by deformation at $90^{o}K$ is always larger than that at $77^{o}K$. This suggests that thermally assisted point defect production takes place during plastic deformation. The only mechanism, which is thermally activable, is the Seeger's jog mechanism mentioned in Section 1.2. Jogs glide easily in the direction of the Burgers vector, and occasionally make non-conservative jumps to create isolated point defects. The rate of thermally activated generation of point defects C_T may be written:

$$\dot{C}_T = \dot{C}_o \, e^{-E_f/KT}, \qquad (3\text{-}14)$$

where E_f is the formation energy of a point defect, K the Boltzmann's constant, $\dot{C}_o$ a constant depending on the jog density. For a given amount of deformation, C_T is proportional to the time, and is

inversely proportional to the strain rate. This is shown schematically in Fig. 3-8a. As mentioned in the previous section, the concentration of point defects produced by the athermal cutting of attractive trees is proportional to the dipole length x formed per intersection event. x increases with the velocity of the moving loop. Although the detailed dependence of x on the velocity is not known, x must have an upper-bound, because it can at most be elongated to the size of the dislocation network. In the actual case, $x << \ell$. Let C_A be the point defect concentration produced by the athermal process, then the total concentration is $C = C_A + C_T$. It is shown schematically in Fig. 3-8b. The experimental data are plotted in Fig. 3-9 and is seen to be in agreement with the theoretical prediction. The overall concentration of point defects produced by deformation at $294^{o}K$ is lower than that produced at $77^{o}K$, because extensive thermal recovery occurs at $294^{o}K$.

The thermally activated jog climb will predominantly generate vacancies because of the lower energy of formation. These extra vacancies are expected to affect the annealing behaviour of point defects. Two specimens deformed to 5% strain with strain rates of 1×10^{-4} and 4×10^{-4} sec^{-1} at $77^{o}K$ were isochronally annealed within the stage III temperature range. The results are shown in Fig. (3-10), (3-11), and (3-12). Both isochronals show two well-defined substages. In heavily deformed copper only a large stage III is observed[47]. Apparently the two substages

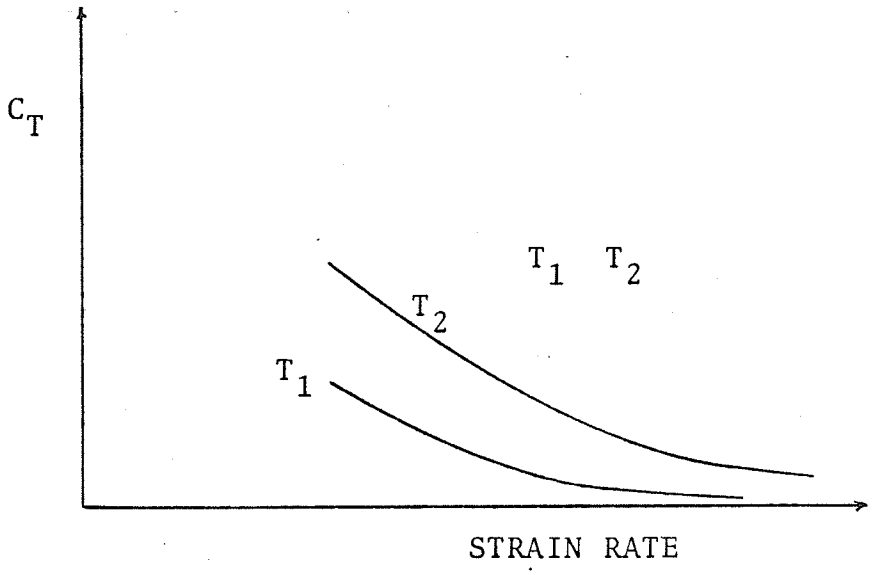

(a)

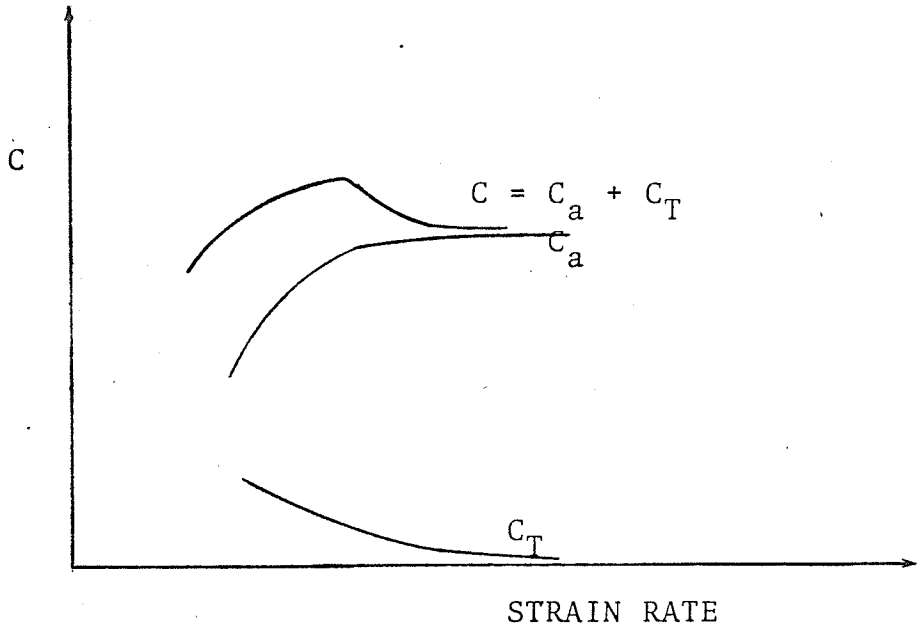

(b)

FIG. 3-8 Thermal and Athermal Production of Point Defects.

FIG. 3-9 Recoverable Resistivity vs. Strain Rate.

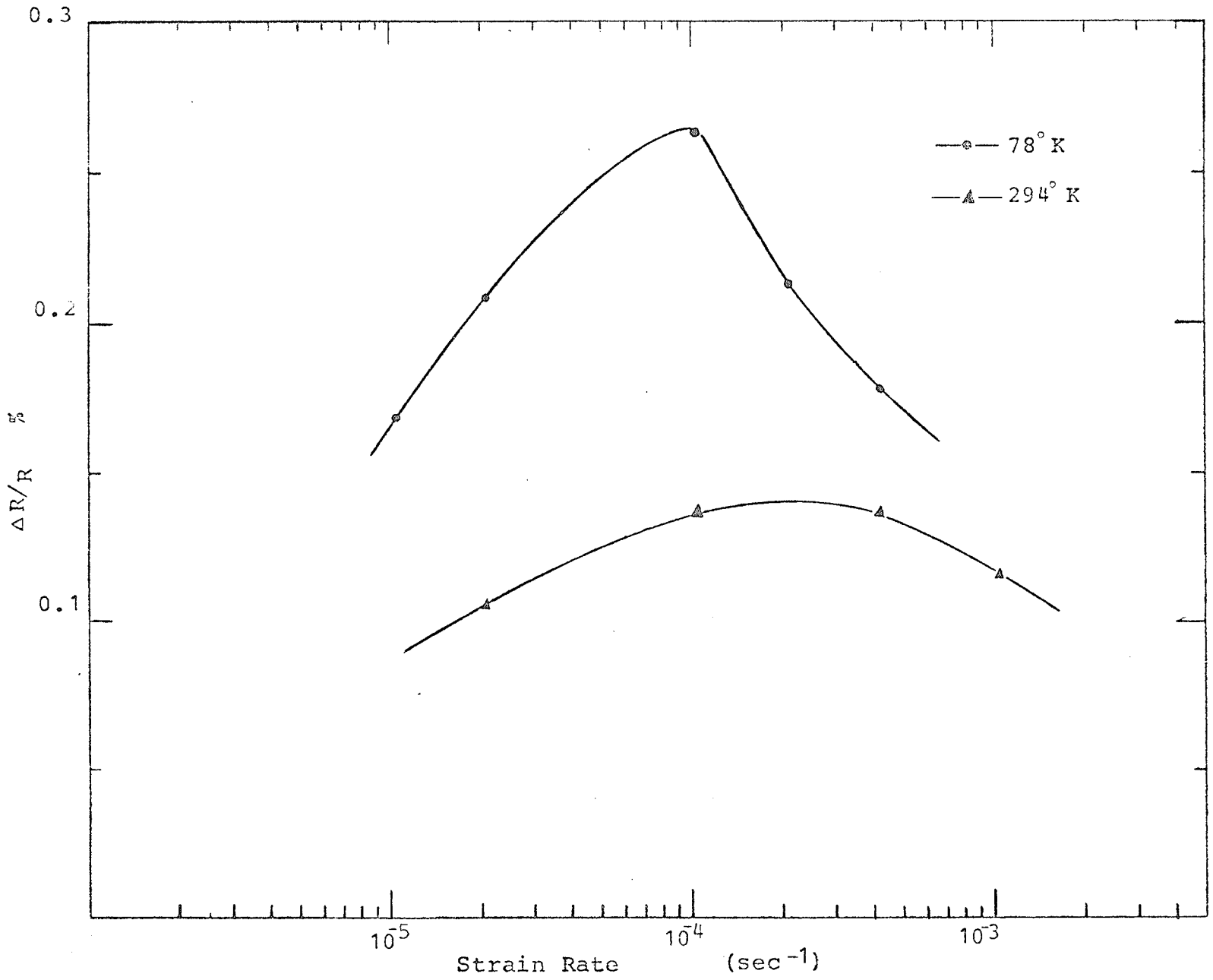

Table 3-2: Recoverable Resistivity vs. Strain Rate

a) Temperature of Deformation = $78^{o}K$

Sp. No.	Crosshead Speed (cm/min)	$\dot{\varepsilon}$ (sec^{-1})	R_1 ($\mu\Omega$)	R_2 ($\mu\Omega$)	R_3 ($\mu\Omega$)	$\Delta R=R_2-R_3$ ($\mu\Omega$)	$\Delta R/R_2$ (%)
35	0.005	1.04×10^{-5}	191.80	212.07	211.71	0.36	0.169
39	0.01	2.08×10^{-5}	190.68	210.79	210.35	0.44	0.209
32	0.05	1.04×10^{-4}	185.18	204.49	203.95	0.54	0.264
38	0.1	2.08×10^{-4}	187.14	206.70	206.26	0.44	0.213
37	0.2	4.16×10^{-4}	191.05	212.91	212.53	0.38	0.178

b) Temperature of Deformation = $294^{o}K$

44	0.01	2.08×10^{-5}	202.84	223.69	223.45	0.24	0.107
36	0.05	1.04×10^{-4}	190.70	210.02	209.73	0.29	0.138
30	0.2	4.16×10^{-4}	190.72	210.32	210.03	0.29	0.138
45	0.5	1.04×10^{-3}	210.28	231.94	231.67	0.27	0.116

R_1 = Resistance before deformation.

R_2 = Resistance after deformation.

R_3 = Resistance after annealed at $170^{o}C$ for 4 hours.

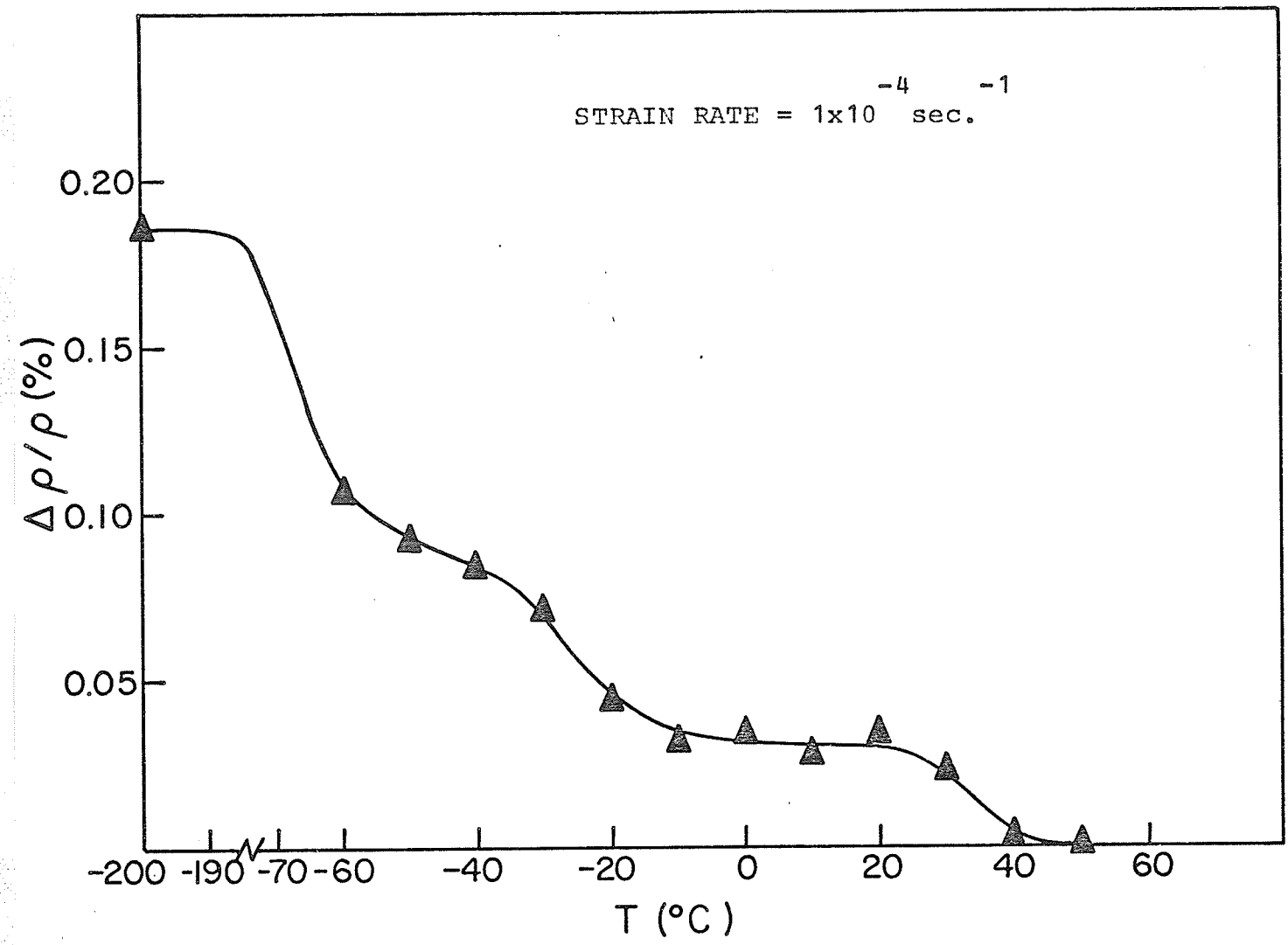

FIG. 3-10 Stage III Recovery.

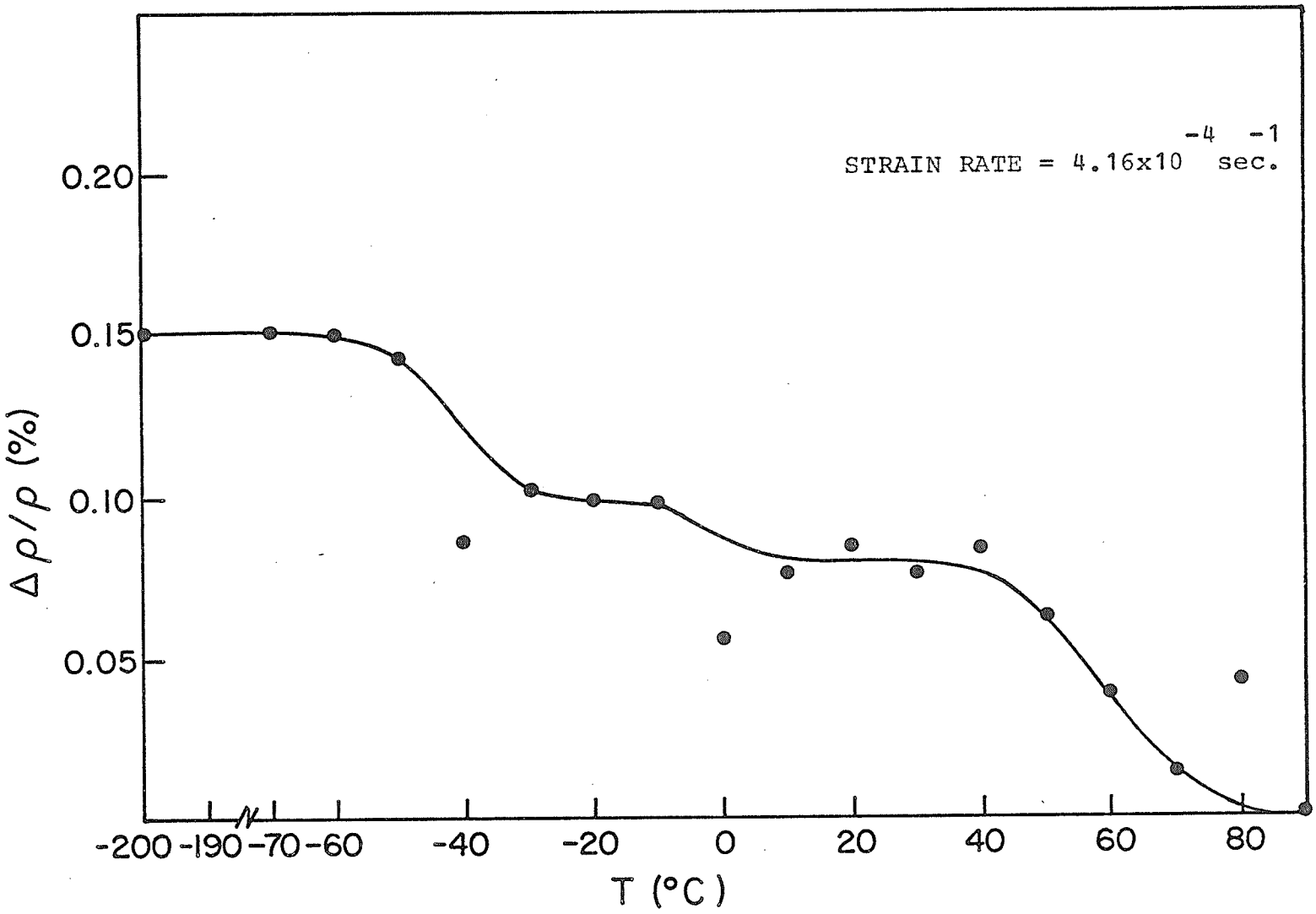

FIG. 3-11 Stage III Recovery.

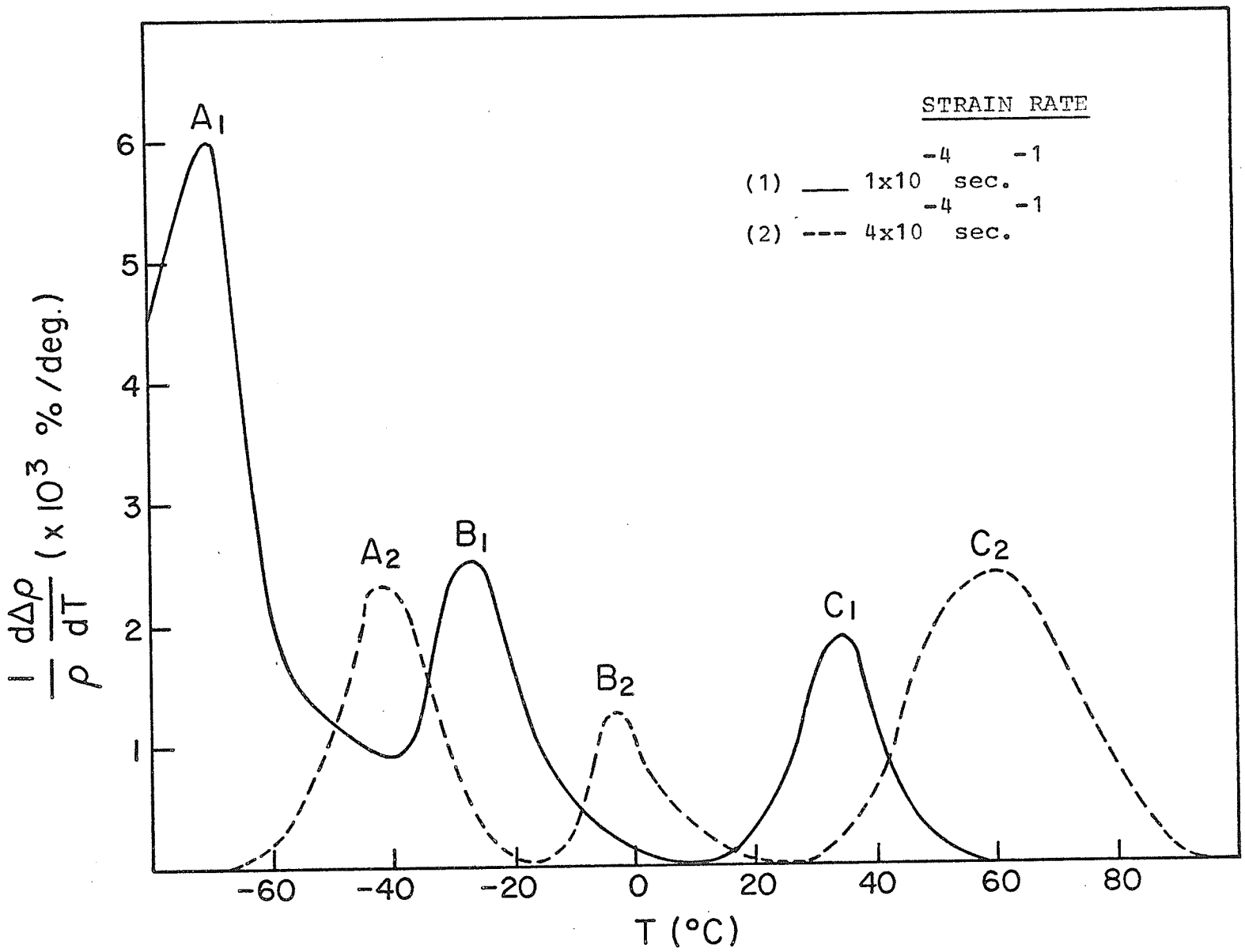

FIG. 3-12 Recovery Spectra of Stage III.

Table 3-3: Isochronal Annealing

Specimen No. 42

Temp. of Deformation = $78^{o}K$

$\varepsilon = 5\%$

$\dot{\varepsilon} = 1x10^{-4}\ sec^{-1}$

5 minutes $10^{o}C$ step

Annealing Temperature (^{o}C)	Resistance ($\mu\Omega$)	Recoverable Resistance ($\mu\Omega$)	Percentage Recovery ($\Delta R/R_{-195}$) %
-195	225.55	0.42	0.186
-60	225.37	0.24	0.106
-50	225.34	0.21	0.093
-40	225.32	0.19	0.084
-30	225.29	0.16	0.071
-20	225.23	0.10	0.044
-10	225.20	0.07	0.031
0	225.21	0.08	0.035
+10	225.19	0.06	0.027
20	225.21	0.08	0.035
30	225.18	0.05	0.022
40	225.14	0.01	0.004
50	225.13	0.00	0.000

Table 3-4: Isochronal Annealing

Specimen No. 49

Temp. of Deformation = $78^{o}K$

$\varepsilon = 5\%$

$\dot{\varepsilon} = 4.16 \times 10^{-4}$ (sec^{-1})

5 minute -10^{o} step

Annealing Temperature (^{o}C)	Resistance ($\mu\Omega$)	Recoverable Resistance ΔR ($\mu\Omega$)	Percentage Recovery $(\Delta R/R_{-195})$ %
-195	235.59	0.38	0.161
-70	235.59	0.38	0.161
-60	235.59	0.38	0.161
-50	235.55	0.34	0.144
-40	235.41	0.20	0.085
-30	235.45	0.24	0.102
-20	235.42	0.21	0.089
-10	235.42	0.21	0.089
0	235.34	0.13	0.055
10	235.39	0.18	0.076
20	235.41	0.20	0.085
30	235.39	0.18	0.076
40	235.41	0.20	0.085
50	235.38	0.17	0.072
60	235.30	0.09	0.038
70	235.24	0.03	0.013
80	235.31	0.10	0.042
90	235.21	0.00	0.000

merge together after large deformation. Although the detailed defects reactions in stage III are not known, the majority of the experimental data (section 1.2.) support the annealing of interstitials. Ramsteiner[79] et al have found that stage III obeys the second order reaction kinetics. They attribute the stage III annealing to the recombination of moving interstitials with vacancies. If this interpretation of the stage III annealing is accepted, the extra vacancies produced by the thermally activated climb of jogs will reduce the mean number of jumps of an interstitial to meet a vacancy. In other words, the average life time of an interstitial will be shortened by the increased vacancy population. The stage III will be shifted to the lower temperature region. The specimen deformed at lower strain rate has higher vacancy concentration. The entire stage III is shifted to the low temperature side with decreasing strain rate (Fig. 3-12).

3.2.3. The Effect of Impurity

Fig. (3-13) shows the total resistivity increase versus strain for Johnson-Matthey and commercial grade (99.96%) copper. The increase in resistivity during deformation is larger for the specimen of lower purity. Buck[75] and Basinski and Saimoto[65] have also found the same effect in single crystal copper. They attribute the larger resistivity increase in low purity copper to the redistribution of impurity atoms. Since it is difficult to differentiate the resistivity changes due to the point defects produced during

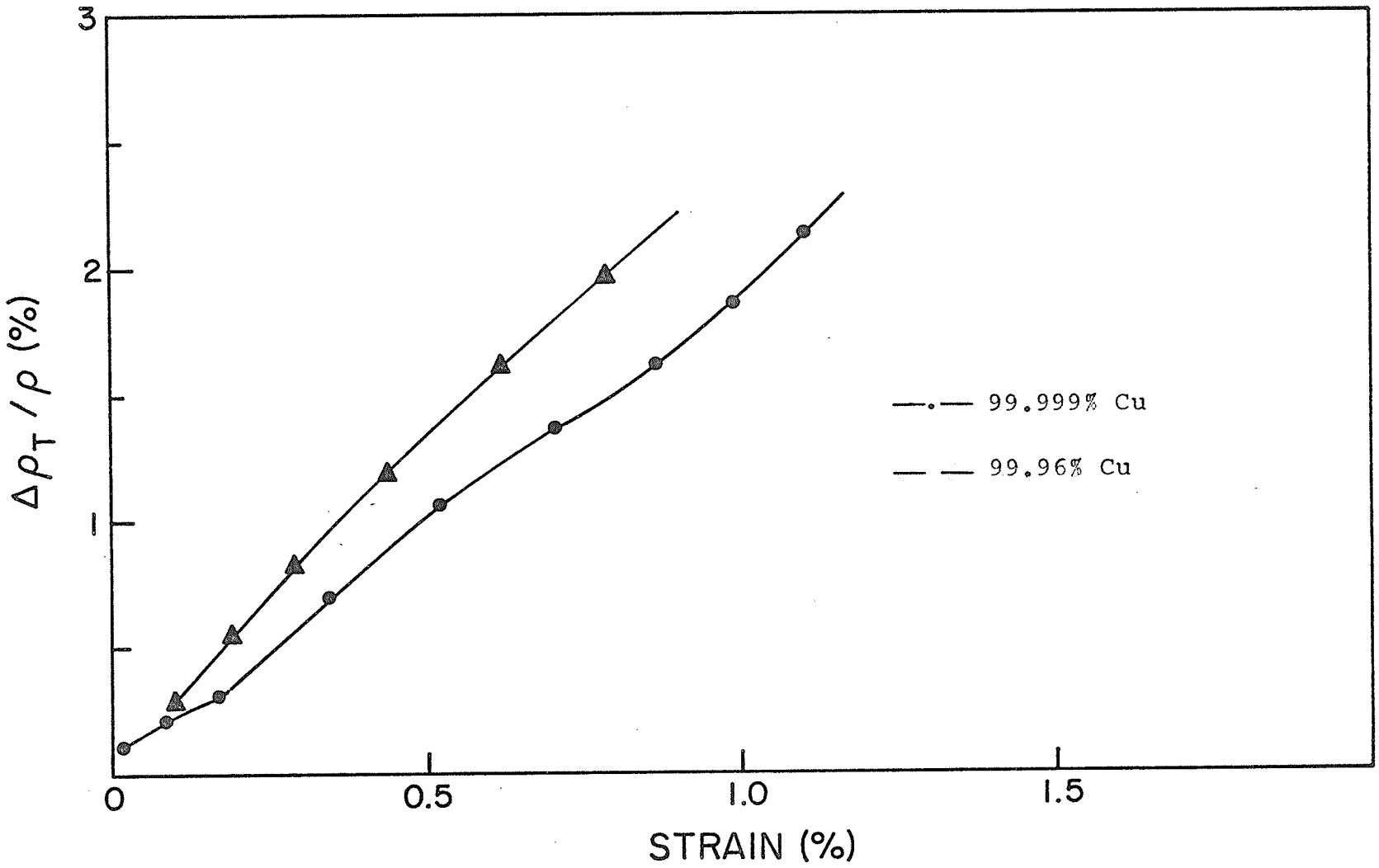

FIG. 3-13 The Effect of Impurity.

deformation and the redistribution of impurity atoms, it is not known whether the impure copper produces more point defects during cold-work. However, it is well-known that impurity atoms can trap point defects to form impurity-point defect complexes if the binding energies are positive. The supersaturation of vacancies produced by cold-work can also enhance the diffusion of impurity atoms. Cu-5 wt% Sn alloy was chosen for the investigation of solute-point defect interaction. This alloy is known to exhibit the Portevin - Le Chatelier effect[73]. This effect is due to the repeated solute locking of dislocations and subsequent generation of new mobile dislocations. It is a diffusion controlled process, and thus depends on the vacancy concentration in the metal. The alloy was deformed to 5% strain and isochronally annealed. The results are shown in Fig. (3-14). The structure of stage III is unchanged by the solute addition. However, there is a large resistivity decrease in the stage IV region. These further conform that the point defects active in stage III are interstitials, and stage IV defects are vacancies. The large resistivity decrease observed in stage IV is apparently due to the redistribution of solute atoms. Only the vacancies can affect the solute diffusion. The extensive solute activity starts at $110^{o}C$. One can also predict that the lowest temperature for the occurrence of the serrated yielding is about $110^{o}C$.

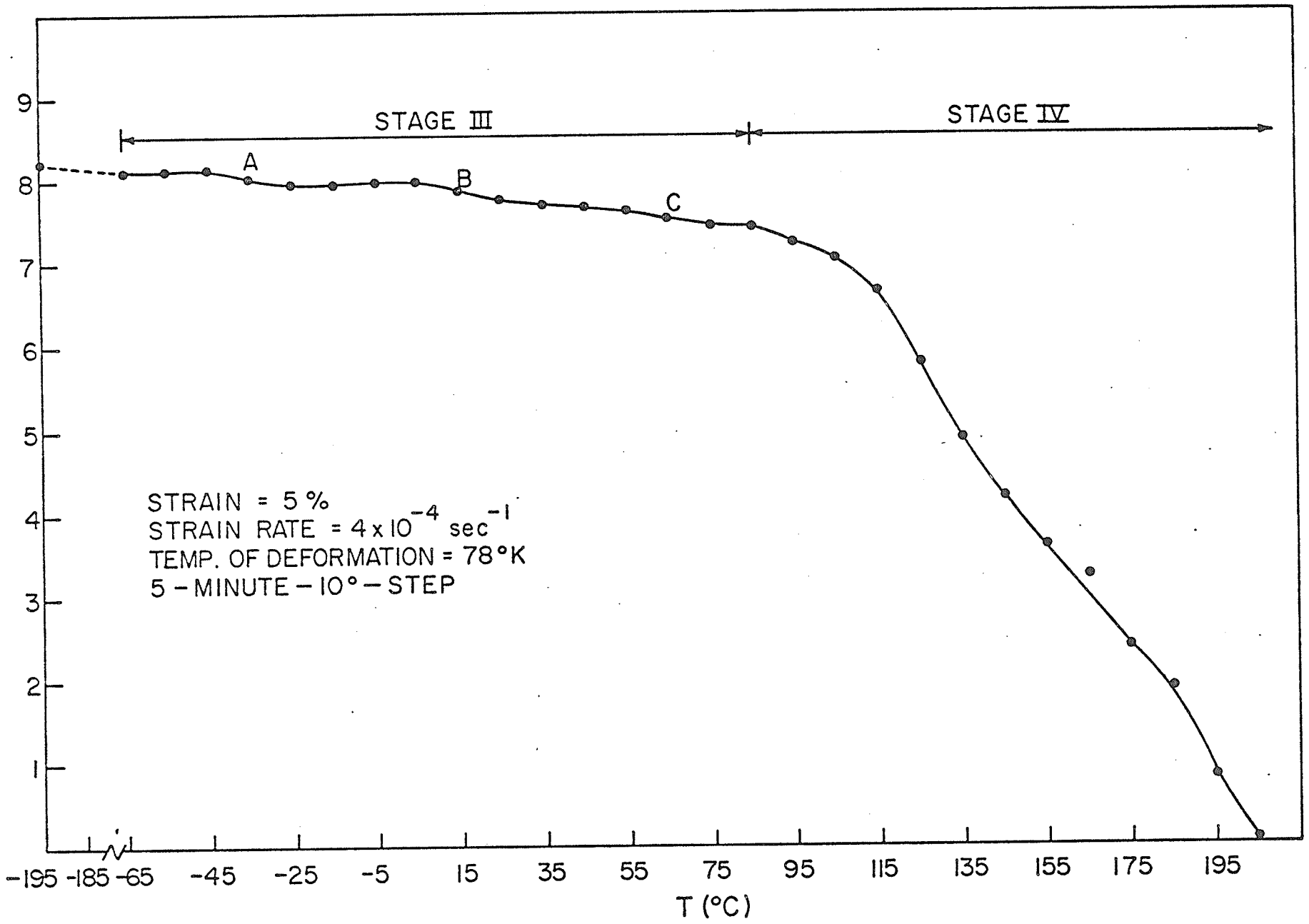

FIG. 3-14 Isochronal Recovery of Cold-worked Cu-5wt%Sn Alloy.

3.3. SUMMARY

1. Saada's model has been re-examined. The length of the point defect string x produced by the athermal cutting of an attractive tree is small compared with the length of the mobile dislocation loop ℓ. x is thus insensitive to the size of the moving loop. However, x increases with increasing dislocation velocity. At a given strain rate, the concentration of point defects produced by the athermal cutting of attractive trees is given by:

$$C_A = \frac{\text{constant}}{\mu^2 b} \int_0^{\varepsilon} \sigma^2 d\varepsilon$$

2. The production of point defects by plastic deformation depends on strain rate as well as temperature of deformation. This suggests that thermally assisted point defect production is not negligible. Seeger's jog mechanism is responsible for the thermally activated production.

3. For copper deformed to a few percent strain, stage III consists of two substages. That is, it involves, at least, two point defects reactions.

4. The structure of stage III is unchanged by the solute addition. There is an extensive solute activity in stage IV. These suggest that the point defects migrating in stage III are interstitials, and stage IV defects are vacancies.

4. REFERENCES

1. A. C. Damask and G. J. Dienes, "Point Defects in Metals", Gordon and Breach, New York, 1971.

2. "Vacancies and Interstitials in Metals", ed. A. Seeger et al, Interscience, 1970.

3. H. B. Huntington, G. A. Shirn and E. S. Wajda, Phys. Rev. 99, 1085, 1955.

4. L. Tewordt, Phys. Rev. 109, 61, 1958.

5. F. G. Fumi, Phil. Mag. 46, 1007, 1955.

6. A. Seeger and H. Bross, Z. Physik 145, 161, 1956.

7. R. O. Simmons and R. W. Balluffi, Phys. Rev. 129, 1533, 1963.

8. J. E. Bauerle, C. E. Klabunde and J. S. Koehler, Phys. Rev. 102, 1182, 1956.

9. J. E. Bauerle and J. S. Koehler, Phys. Rev. 107, 1493, 1957.

10. F. J. Bradshaw and S. Pearson, Phil. Mag. 2, 379 and 570, 1957. Also Phil. Mag. 1, 812, 1956.

11. B. G. Lazarev and O. N. Ovcharenko, Kokl. Akad. Nauk SSSR, 100, 875, 1955.

12. W. DeSorbo, Phys. Rev. 117, 444, 1960.

13. J. Takamura, Acta Met 9, 547, 1961.

14. T. Mori, M. Meshii and J. W. Kauffman, J. Appl. Phys. 33, 2776, 1962.

15. R. P. Huebener and C. G. Homan, Phys. Rev. 129, 1162, 1963.

16. J. S. Koehler, in reference 2, page 169.

17. G. L. Bacchella, E. Germagnoli and S. Granata, J. Appl. Phys. 30, 570 and 748, 1959.

18. W. Bauer and W. F. Goeppinger, Phys. Rev. 154, 588, 1967.

19. J. J. Jackson, in "Lattice Defects in Quenched Metals", ed.

Cotterill et al, Academic Press, New York, 1965, page 467.

20. M. Doyama and J. S. Koehler, Phys. Rev. 127, 21, 1962.

21. L. J. Cuddy and E. S. Machlin, Phil. Mag. 7, 745, 1962.

22. Y. J. Quéré, J. Phys. Soc. Japan 18, Suppl. III, 91, 1963.

23. O. N. Ovcharenko, Phys. Metals Metallog. 11, 78, 1961.

24. W. DeSorbo and D. Turnbull, Acta Met 7, 83, 1959.

25. R. L. Chaplin and H. M. Simpson, Phys. Rev. 163, 587, 1967.

26. H. Kimura, A. Kimura and R. R. Hasiguti, Acta Met 10, 607, 1962.

27. J. Bass, Phil. Mag. 15, 717, 1967.

28. G. Airoldi, G. L. Bacchella and E. Germagnoli, Phys. Rev. Letters 2, 145, 1959.

29. C. Budin, F. Denayrow, A. Lucasson and P. Lucasson, Compt. Rend. Acad. Sci. Paris, 256, 1518, 1963.

30. P. Wright and J. H. Evans, Phil. Mag. 13, 521, 1966.

31. S. Scherrer, G. Lozes and B. Deviot, Jülich Conf., 1968, Vol. I, page 167.

32. W. DeSorbo, J. Phys. Chem. Solids 15, 7, 1960.

33. C. J. Beevers, Acta Met 11, 1029, 1963.

34. R. M. Cotterill, Phil. Mag. 6, 1351, 1961.

35. C. P. Flynn, J. Bass and D. Lazarus, Phil. Mag. 11, 521, 1965.

36. S. D. Gertsriken and N. N. Novikov, Phys. Metals Metallog. 9, 54, 1960.

37. C. Panseri and T. Federighi, Phil. Mag. 3, 1223, 1958.

38. J. W. Corbett, R. B. Smith and R. M. Walker, Phys. Rev. 114, 1452 and 1460, 1959.

39. G. W. Iseler, H. I. Dawson and J. W. Kauffman, in "Lattice Defects and their Interactions", ed. R. R. Hasiguti, Gordon and Breach, New York, 1967, page 654 and 681.

40. A. Sosin and K. R. Garr, Phys. Rev. 161, 664, 1967.

41. C. J. Meechan, A. Sosin and J. A. Brinkman, Phys. Rev. 120, 411, 1960.

42. J. W. Corbett, in reference 2, page 977.

43. C. W. Berghout, Acta Met 4, 211, 1956.

44. K. R. Garr and A. Sosin, Phys. Rev. 162, 669, 1967.

45. U. Gonser, in reference 2, page 649.

46. A. Seeger and F. J. Wagner, Phys. Stat. Sol. 9, 583, 1965.

47. A. van den Beukel, in reference 2, page 427.

48. F. Seitz, Advances in Phys. 1, 43, 1952.

49. A. Seeger, Phil. Mag. 46, 1194, 1955.

50. G. Saada, in "Electron Microscopy and Strength of Crystals", ed. G. Thomas, Wiley, 1962, page 651.

51. A. Seeger, in "Theory of Crystal Defects", ed. B. Gruber, Academic Press, 1966, page 37.

52. H. B. Aaron and H. K. Birnbaum, Acta Met 13, 205, 1965.

53. H. K. Birnbaum, J. Appl. Phys. 34, 2175, 1963.

54. H. Kronmüller, in reference 2, page 667.

55. M. L. Swanson, Phys. Stat. Sol. 3a, 287 and 551, 1970.

56. D. Schumacher and A. Seeger, Phys. Letters 7, 184, 1963.

57. A. Seeger, P. Schiller and H. Kronmüller, Phil. Mag. 5, 853, 1960.

58. C. W. Berghout, Acta Met 6, 613, 1958.

59. R. W. Balluffi, J. S. Koehler and R. O. Simmons, in "Recovery and Recrystallization of Metals", ed. L. Himmel, Interscience, New York, 1962, page 1.

60. H. I. Dawson, Acta Met 13, 453, 1965.

61. J. Molenaar and W. H. Aarts, Nature, 166, 690, 1950.

62. M. J. Druyvesteyn and J. A. Manintveld, Nature 168, 868, 1951.

63. W. R. Hibbard Jr., Acta Met 7, 565, 1959.

64. R. H. Pry and R. W. Hennig, Acta Met 2, 318, 1954.

65. Z. S. Basinski and S. Saimoto, Canad. J. Phys. 45, 1161, 1967.

66. H. R. Peiffer, J. Appl. Phys. 34, 298, 1963.

67. In reference 1, page 173.

68. K. Rösch, F. Bell and R. Sizmann, "Int. Conf. on Vacancies and Interstitials", Jülich, 1968, page 444.

69. J. S. Dugdale and Z. S. Basinski, Phys. Rev. 157, 552, 1967.

70. J. Friedel, "Dislocations", Addison-Wesley, Reading, 1964.

71. A. Kapicka and J. Polak, Czech. J. Phys. B22, 476, 1972.

72. In reference 70, page 123.

73. D. J. Lloyd and P. J. Worthington, Phil. Mag. 24, 195, 1971.

74. W. H. Aarts and R. K. Jarvis, Acta Met 2, 87, 1954.

75. O. Buck, Phys. Stat. Sol. 2, 535, 1962.

76. H. I. Dawson, Ph.D. Thesis, Delft, 1964.

77. H. I. Dawson, Physica 31, 1046, 1965.

78. In reference 70, page 116.

79. F. Ramsteiner, W. Schüle and A. Seeger, Phys. Stat. Sol. 7, 937, 1964.

80. J. W. Corbett, in "Electron Irradiation Damage in Semiconductors", Academic Press, New York, 1966.

81. C. L. Snead, F. W. Wiffen and J. W. Kauffman, Phys. Rev. 164, 900, 1967.

82. D. L. Dexter, Phys. Rev. 103, 107, 1956.

83. W. Schilling, G. Burger, K. Isebeck and H. Wenzl, in reference 2, page 255.

84. R. N. Singh, Thesis, University of Manitoba, 1969, and R. N. Singh and K. Tangri, unpublished results.

85. A. Sosin and H. H. Neeley, Phys. Rev. 127, 1465, 1962.

86. P. Jongenburger and H. G. van Bueren, "Imperfections in Crystals", North-Holland, 1961.

87. J. Price, J. Appl. Phys. 32, 1750, 1961.

88. J. Takamura, K. Furukawa, S. Miura, and P. H. Shingu, J. Phys. Soci. Japan, 18, Suppl. III, 7, 1963.

89. D. Kuhlmann-Wilsdorf, in "A.S.M. Symp. on Strengthening Mechanisms in Solids", 1962, page 137.